Topoisomerases modulate the timing of meiotic DNA breakage and repair

Jonna Heldrich [1], Xiaoji Sun [1,2], Luis A. Vale-Silva [1,3], Tovah E. Markowitz [1,4], and Andreas Hochwagen [1,*]

[1] Department of Biology; New York University; New York, NY 10003, USA

[2] Current address: Cellarity Inc., Cambridge, MA, USA.

[3] Current address: BioQuant Center, Heidelberg University, Heidelberg, Germany.

[4] Current address: Frederick National Laboratory for Cancer Research, Frederick, MD, USA.

* Lead contact and corresponding author (andi@nyu.edu)

Running title: Topoisomerases in meiotic prophase

Abstract

During meiotic prophase, concurrent transcription, recombination, and changes in chromosome morphology place substantial topological strain on chromosomal DNA, but the roles of topoisomerases in this context remain poorly defined. Here, we show that meiotic *Saccharomyces cerevisiae* chromosomes accumulate topoisomerases primarily in promoter-containing intergenic regions (IGRs) of actively transcribing genes. Wide IGRs exhibit the highest level of meiotic transcription and the strongest topoisomerase buildup. Topoisomerase binding partially overlaps with double-strand break (DSB) hotspots, where the topoisomerase-like enzyme Spo11 initiates meiotic recombination. We show that *TOP1* disruption mildly delays DSB induction, whereas a catalytic loss-of-function allele of *TOP2* (*top2-1)* accelerates DSB formation. This acceleration is associated with persistent Top2 on meiotic chromosomes and is not observed upon Top2 depletion. In addition to altering DSB timing, the *top2-1* allele also uncouples chromosome synapsis from Pch2/TRIP13-dependent chromosome remodeling and delays DSB repair. Thus, topoisomerase function is required at multiple points to modulate the timing of meiotic recombination.

Meiosis/topo I/topo II/ synaptonemal complex/Hop1

Introduction

Topoisomerases preserve genome integrity by resolving topology-related strain and DNA entanglements associated with many cellular processes, including replication, transcription, and recombination (Pommier et al, 2016; Vos et al, 2011; Wang, 2002). To resolve strain, topoisomerases catalyze temporary breaks in the DNA. Type I topoisomerases make and re-ligate a single-strand break to allow swiveling of the DNA substrate, whereas type II enzymes catalyze DNA strand passage through a transient double-strand break (DSB). Topoisomerases are major chemotherapeutic targets that have been extensively studied in mitotically proliferating cells (Pommier et al, 2016). Comparatively less is known about the function of topoisomerases during meiosis.

Meiosis is a specialized type of cell division that is essential for sexual reproduction and allows for generation of genetic diversity. Meiosis involves a single round of DNA replication followed by two divisions that separate homologous chromosomes and sister chromatids, respectively, to produce four haploid cells from one diploid cell. In preparation for the first meiotic division, programmed DSB formation initiates exchange of DNA between homologous chromosomes by meiotic recombination (Borde & de Massy, 2013; Lam & Keeney, 2015a). This process allows for shuffling of genetic information and leads to the formation of crossovers, which help promote proper segregation of homologous chromosome pairs (Petronczki et al, 2003). Errors in this process can result in aneuploidy, infertility and congenital diseases, such as Down syndrome (Hassold & Sherman, 2000).

To support meiotic recombination, meiotic chromosomes assemble conserved loop-axis structures on actively transcribing chromatin, culminating in the formation of the synaptonemal complex (SC) between pairs of homologous chromosomes (Sun et al,

2015; Zickler & Kleckner, 2015). The SC limits DSB induction and promotes rapid repair of meiotic DSBs before cells exit from meiotic prophase and initiate the first meiotic division (Subramanian et al, 2016; Thacker et al, 2014). Chromosome morphogenesis, transcription, and recombination take place concurrently during meiotic prophase and are expected to place substantial topological strains on prophase DNA.

The meiotic functions of topoisomerases have been primarily elucidated in the context of the meiotic divisions where, similar to mitosis, topo II has a major role in disentangling DNA to facilitate chromosome segregation (Gomez et al, 2014; Hartsuiker et al, 1998; Hughes & Hawley, 2014; Jaramillo-Lambert et al, 2016; Kallio & Lahdetie, 1996; Mengoli et al, 2014; Tateno & Kamiguchi, 2001). However, both topoisomerases are also present and active in meiotic prophase (Borde et al, 1999; Cobb et al, 1997; Stern & Hotta, 1983). Only minor meiotic defects have been reported upon inactivation of topo I, including increased gene conversion events in the ribosomal DNA of *S. cerevisiae* (Christman et al, 1988) and mild defects in chromosome pairing in mice (Cobb et al, 1997; Handel et al, 1995). Somewhat more is known about topo II, which localizes diffusely to prophase chromatin in a variety of organisms (Cheng et al, 2006; Cobb et al, 1999; Jaramillo-Lambert et al, 2016; Zhang et al, 2014), with enrichment along chromosome axes noted in some cases (Klein et al, 1992; Moens & Earnshaw, 1989). In *Saccharomyces cerevisiae*, topo II contributes to proper spacing of crossover events (Zhang et al, 2014). Aberrant recombination upon chemical inhibition of topo II has also been noted in mouse spermatocytes (Russell et al, 2000). In addition, topo II helps resolve chromosome interlocks in *Arabidopsis* (Martinez-Garcia et al, 2018). Possibly related to this function, *Saccharomyces cerevisiae* topo II mutants arrest at the end of meiotic prophase in a DSB-dependent manner despite the appearance of mature recombinants (Rose & Holm, 1993; Rose et al, 1990; Zhang et al, 2014). However, an

in-depth analysis of topoisomerase distribution on prophase chromosomes has so far not been performed.

In this study, we used chromatin immunoprecipitation and deep sequencing to determine the meiotic distribution of topoisomerases I and II (encoded by *TOP1* and *TOP2*) in *S. cerevisiae*. We show that both topoisomerases are primarily enriched in promoter-containing intergenic regions (IGRs) and that enrichment correlates with transcriptional activity and increases upon meiotic entry. We find that topoisomerase binding only imperfectly overlaps with sites of DSB formation, even though Spo11, the enzyme catalyzing meiotic DSBs, belongs to the topo II family. Nevertheless, disruption of *TOP1* and *TOP2* alters the timing of meiotic DSB formation. In addition, mutation of *TOP2* leads to defects in meiotic DSB repair and chromosome axis morphogenesis, and we present evidence that these defects are caused by the binding of inactive Top2 protein.

Results

Topoisomerases are enriched at sites of meiotic DSB formation

To investigate the potential sites of topological stress during meiotic prophase, we examined the chromosomal association of yeast Top1 and Top2 in a synchronous meiotic time course. Immunofluorescence analysis of chromosome spreads showed that both proteins form foci on chromatin that are detectable at all stages of meiotic prophase as well as prior to meiotic induction (**Figures S1A-B**). As chromosomes compact to form the synaptonemal complex (SC), Top1-13myc and Top2 are detectable both on chromatin loops and in the vicinity of the chromosome cores, as marked by the SC protein Zip1. Both proteins, especially Top1-13myc, are also present in the nucleolus, which is devoid of Zip1 staining (arrowhead, **Figure S1A**).

To obtain more detailed spatial information, we analyzed the genomic distribution of Top1 and Top2 by chromatin immunoprecipitation and deep sequencing (ChIP-seq) at the time of maximal meiotic DSB formation (3h after meiotic induction). This analysis showed that Top1 and Top2 bind in a similar pattern (**Figure 1A**), which presumably reflects the genomic distribution of topological stress. Metagene analysis showed a particular enrichment upstream of gene bodies in promoter regions (**Figure 1B**), consistent with analyses of Top2 in vegetative cells (Bermejo et al, 2007; Gittens et al, 2019; Sperling et al, 2011). The enrichment downstream of ORFs is a consequence of the promoter of the next gene. When signals were parsed into divergent, tandem, and convergent intergenic regions (IGRs), topoisomerase enrichment was only observed in IGRs containing at least one promoter, with the strongest signal observed for divergent IGRs (**Figure 1C, Figure S1C**). Both topoisomerases are broadly bound in the intergenic space delimited by the two flanking genes (**Figure 1D-E**), although

topoisomerase enrichment appeared comparatively reduced in narrow IGRs (**Figure 1F-G**), suggesting that IGR size may influence topoisomerase recruitment.

Topoisomerase binding correlates with transcriptional activity

We tested whether meiotic topoisomerase enrichment in IGRs is linked to the transcriptional activity of the flanking genes by performing RNA-seq analysis 3h after meiotic induction. This analysis revealed a direct correlation between topoisomerase binding and gene expression levels (**Figure 2A-B**). The correlation was strongest in promoter regions but extended across ORFs for the most highly expressed quartile, consistent with increased buildup of topological stress on highly expressed genes (Teves & Henikoff, 2014). We also observed an increase in topoisomerase association downstream of highly expressed ORFs. This association may reflect topological stress in the 3' UTRs or the fact that neighboring genes in the yeast genome are sometimes co-regulated (Cohen et al, 2000; Swygert et al, 2019).

Unexpectedly, transcriptional activity in meiosis appears strongly associated with the size of divergent IGRs. Comparing divergent IGR sizes as a function of transcription showed that gene pairs in which both genes are among the most highly expressed have nearly twice as large of an IGR than gene pairs in which both genes are among the most lowly expressed (**Figure 2C**). This bias likely accounts for the broader topoisomerase distribution in the most highly transcribed quartile (**Figure 2A-B**). Tandem IGRs did not show this bias (**Figure 2C**), indicating that this feature is linked to relative gene arrangement. We confirmed this association by analyzing recently published RNA-seq time course data (Cheng et al, 2018). This analysis showed that highly expressed gene pairs are preferentially associated with large divergent IGRs throughout meiosis but not in proliferating cells (**Figures 2D and S2**). The effect is already seen prior to meiotic

entry and in non-meiotic *MATa/a* cells in sporulation media, suggesting that it is linked to the starvation regime used to induce synchronous meiosis in yeast. This bias in transcriptional activity may also contribute to the apparently lower enrichment of topoisomerases in narrow IGRs (**Figure 1F-G**).

Meiotic entry leads to a buildup of Top2 in promoter-containing IGRs

To test if meiotic chromosome morphogenesis impacts topoisomerase recruitment, we followed Top2 enrichment as cells transition from pre-meiotic G1 into meiotic prophase using spike-in normalized ChIP-seq analysis (SNP-ChIP (Vale-Silva et al, 2019)). This analysis showed an overall ~40% increase in Top2 binding across the genome and in convergent IGRs (**Figure 3A,D**) and a nearly 2.5-fold increase in promoter-containing IGRs (**Figure 3E**). This increase occurred regardless of IGR size, indicating that it is not linked to transcriptional changes (**Figure 3B-C**). These data indicate that promoter-containing IGRs experience a substantial buildup of topological stress as cells enter meiotic prophase. Meiotic DSB hotspots also occur preferentially in promoter-containing IGRs where they are catalyzed by the topoisomerase II-related protein Spo11 (Lam & Keeney, 2015b; Pan et al, 2011). Interestingly, meiotic DSB hotspots experience an even stronger buildup of Top2 than average promoter-containing IGRs (**Figure 3F**).

Topoisomerase enrichment is correlated with meiotic DSB hotspot activity

The buildup of Top2 at DSB hotspots prompted us to investigate the link between topoisomerase binding and Spo11 activity. To compare topoisomerase binding and hotspot activity, we reanalyzed high-resolution sequencing data of Spo11-associated oligonucleotides (Spo11-oligos), which report on Spo11 cleavage activity (Pan et al, 2011; Thacker et al, 2014). Consistent with previous work (Blitzblau et al, 2007; Gittens et al, 2019), Spo11-oligo signal is strongest in the promoter regions of highly expressed

genes (**Figure 4A**). Similar to topoisomerase binding, we also noted somewhat increased Spo11 activity downstream of highly expressed genes (**Figure 4A**). However, in other aspects Spo11 cleavage patterns differed from the patterns observed for topoisomerase association. First, the association with transcriptional activity was less pronounced than for topoisomerases (**Figures 2A-B, 4A**). Second, Spo11 cleavage activity is more focused, and more closely overlaps the regions of nucleosome depletion (**Figure 4B-C**) (Pan et al, 2011). Third, Spo11 activity is not biased toward large IGRs (**Figure 4B**). We note that some of these differences may due to the differences in assays, as Spo11-oligos map precise cleavage sites, whereas ChIP-seq analysis maps broader regions of association based on formaldehyde crosslinking. Nonetheless, these observations argue against a shared mechanism driving enrichment of topoisomerase recruitment and Spo11 activity.

It is possible that the topoisomerases and Spo11 respond similarly to the local chromatin environment at IGRs. Indeed, when we analyzed relative topoisomerase enrichment after splitting DSB hotspots into quantiles based on Spo11 activity, we observed a significant correlation between Top1 and Top2 enrichment and Spo11 activity based on 95% confidence intervals (**Figure 4D**). To further probe this link, we conducted the inverse analysis. We compared the average Spo11 activity of hotspots overlapping with a strong peak of Top1 or Top2 with those that did not (**Figure 4E**). This analysis showed that DSB hotspot activity is elevated at hotspots that exhibit significant Top2 enrichment. The additional presence of Top1 does not significantly increase the activity of Top2-enriched hotspots. Top1 enrichment at hotspots is not correlated with hotspot activity, suggesting that Top1 and Top2 interact differently with DSB hotspots.

Opposing effects of *TOP1* and *TOP2* on DSB timing

To test if the enrichment of Top1 and Top2 at meiotic DSB hotspots has functional consequences for the induction of meiotic recombination, we monitored meiotic DSB activity in cells in which either topoisomerase has been inactivated. After collecting DNA from a synchronous meiotic time course, we analyzed the dynamics of DSBs by pulsed field gel electrophoresis (PFGE) followed by Southern blotting for chromosome VIII. In order to analyze accumulation of DSBs, we used mutants with a *dmc1Δ* background, which are unable to repair DSBs. Flow cytometry analysis showed that *top1Δ* mutants underwent pre-meiotic DNA replication with wild-type kinetics (**Figure 5A**). However, the appearance of meiotic DSB bands was mildly delayed (**Figure 5B-C**). These data indicate that Top1 is required, directly or indirectly, for the timely initiation of Spo11 catalysis.

To assess the role of Top2 in DSB formation, we used the thermo-sensitive *top2-1* mutant to conditionally inactivate Top2 protein (DiNardo et al, 1984). For experiments utilizing this mutant, wild type and mutant cells were induced to enter meiosis at room temperature and then shifted to 34°C one hour after meiotic induction. Flow cytometry analysis of *top2-1* showed delayed entry into meiosis compared to control cells (**Figure 5D**). Despite this delay, DSB formation in *top2-1 dmc1Δ* cells initiated earlier than in control cells (**Figure 5E-F**). Early break formation was also apparent when analyzing DSB hotspots in the promoters of *CCT6* and *CPA2* by standard gel electrophoresis and Southern blotting (**Figure S3A-B**). No breaks were observed in *top2-1* mutants lacking *SPO11* (**Figure S3C**), indicating that accelerated DSB formation is not the result of breaks arising because of defects in DNA replication. These data indicate that the two topoisomerases have non-redundant roles in modulating meiotic DSB timing.

Top2 inactivation delays meiotic DSB repair

We further assessed the effects of topoisomerase inactivation by analyzing repair-competent (*DMC1*) cells. PFGE/Southern analysis of chromosome VIII recapitulated delayed DSB induction in *top1Δ* mutants (**Figure S4A**) and early initiation of DSB formation in *top2-1* mutants (**Figure 6A)**. DSBs disappeared with normal kinetics in *top1Δ* mutants, suggesting largely normal DSB repair (**Figure S4A**). By contrast, DSBs in the *top2-1* mutant persisted late into meiosis after wild type cells had completed DSB repair. In part, the delay of the mutant is explained by the poorer synchrony and delayed completion of premeiotic S phase (**Figure 5D**). However, the delay could also indicate an additional defect in meiotic DSB repair.

To better understand the effects of the *top2-1* mutant, we analyzed the chromosomal association of mutant Top2 protein during meiosis. Immunofluorescence staining for Top2 on chromosome spreads showed foci localizing abundantly to meiotic chromosomes in the *top2-1* mutant (**Figure 6B)**, demonstrating that despite a loss of catalytic activity above 30°C (DiNardo et al, 1984), the mutant Top2 protein retains the capacity to bind to meiotic chromosomes. The local distribution of Top2 is altered, however, because ChIP-seq analysis in *top2-1* mutants revealed a loss of Top2 binding from promoter regions (**Figure 6C-D**). Interestingly, mutant Top2 appeared to persist at sites overlapping with the meiotic chromosome axis factor Red1.

We wondered whether the persistent binding of mutant Top2 could be responsible for the observed DSB kinetics of the *top2-1* mutant. To test this possibility, we depleted Top2 using the anchor away technique, which allows conditional nuclear depletion of FRB-tagged proteins upon addition of rapamycin (Haruki et al, 2008; Subramanian et al, 2016). Depletion of Top2-FRB upon meiotic induction (0h) did not interfere with premeiotic S phase (**Figure S4B**) and led to a near complete removal of Top2 from

chromosomes as assayed by immunofluorescence of chromosome spreads (**Figure 6E**). PFGE/Southern analysis showed that, unlike the *top2-1* mutant, Top2 depletion did not lead to accelerated DSB induction (**Figure 6F**), suggesting that this phenotype is linked to the binding of mutant Top2 to chromosomes. However, quantification of the major DSB bands revealed that DSB signal was reproducibly elevated upon Top2 depletion (**Figure S4C**). This increase likely reflects delayed DSB repair kinetics because DSB levels were unaffected when Top2 depletion was analyzed in a *dmc1Δ* mutant background (**Figure S4D-E**). Delayed repair kinetics upon Top2 depletion was also observed previously at the *HIS4LEU2* model recombination hotspot (Zhang et al, 2014).

Persistent Top2 interferes with synapsis-associated chromosome remodeling

Given the important role of chromosome structure in guiding meiotic DSB repair (Zickler & Kleckner, 2015), we asked whether some of the repair defects of *top2* mutants could be related to defects in chromosome morphogenesis. To assay meiotic chromosome structure, we stained chromosome spreads for the structural components Hop1 and Zip1. Hop1 is recruited to chromosomes prior to DSB formation and is removed at the time of repair, as the SC component Zip1 is deposited onto the chromosomes (Smith & Roeder, 1997; Subramanian et al, 2016). As a result, Hop1 and Zip1 show a complementary pattern on wild-type chromosomes (**Figure 7A**). By contrast, Hop1 and Zip1 signals exhibit substantial overlap on *top2-1* chromosomes (**Figure 7A)**. Furthermore, DAPI staining of *top2-1* mutants revealed the accumulation of chromosomes with characteristic parallel “train tracks”, which rarely appear in wild-type nuclei (**Figure 7B**). Overlapping Hop1 and Zip1 signals and DAPI train tracks are indicative of a defect in proper Hop1 removal and a hallmark of mutants that fail to recruit the AAA+ ATPase Pch2 (Borner et al, 2008; San-Segundo & Roeder, 1999; Subramanian et al, 2016; Subramanian et al, 2019). Indeed, analysis of Pch2

recruitment in the *top2-1* mutant across a meiotic time course revealed that whereas nucleolar binding occurred normally, Pch2 binding along chromosomes was uncoupled from SC formation and only occurred with a substantial delay (**Figure 7C**). These data indicate that Top2 is involved in coupling Pch2 recruitment and Hop1 removal to the assembly of the SC.

To test whether lack of activity or binding of the mutant Top2 conferred these phenotypes to *top2-1* mutants, we analyzed chromosome spreads of cells depleted for Top2-FRB by anchor away. In these cells, Hop1 and Zip1 distribution as well as DAPI staining patterns were indistinguishable from wild type (**Figure 7A-B**). These data indicate that the uncoupling of SC assembly and chromosome remodeling is the result of persistent binding of inactive Top2.

Discussion

Topoisomerases are essential for protecting the genome from topological stress associated with most aspects of DNA metabolism, including DNA replication, transcription, and chromosome segregation. Here, we show that topoisomerases are involved in the DNA processes associated with meiotic recombination and modulate the timing of meiotic DSB formation and repair.

Our data show that similar to vegetative cells, topoisomerases are strongly enriched in IGRs, suggesting an accumulation of topological stress in these regions. Top2 primarily builds up in large IGRs, which, unexpectedly, are also strongly associated with high levels of meiotic gene expression. Two observations, however, argue against the model that Top2 buildup in wide IGRs is solely a consequence of this increased transcription. First, analyses in vegetative cells found no link between Top2 activity and transcription of the flanking genes (Gittens et al, 2019). Second, Top2 builds up as cells enter meiotic prophase, whereas elevated transcription in wide IGRs is already seen in premeiotic cells. These observations imply an additional source of topological stress. An obvious candidate is the assembly of the axial element, which occurs specifically in meiotic prophase. Additional stress may also arise from the starvation conditions needed to induce meiosis; indeed, nutrient depletion leads to substantial chromatin compaction in yeast (Rutledge et al, 2015). Notably, both axial element assembly and starvation-associated chromatin compaction require the chromosome remodeler condensin (Pommier et al, 2016; Swygert et al, 2019; Yu & Koshland, 2003), which frequently acts in conjunction with Top2. We therefore speculate that the combined topological stresses from changes in chromosome structure and transcription drive topoisomerase buildup at wide IGRs.

Spo11, the conserved enzyme responsible for meiotic DSB formation, is structurally related to type II topoisomerases and is also most active in IGRs (Baudat & Nicolas, 1997; Pan et al, 2011). Despite these similarities, our data indicate clear spatial differences in topoisomerase binding and Spo11 activity, arguing against a shared recruitment mechanism. These binding differences do not exclude the possibility that Spo11 also responds to DNA topology, as topological stress can propagate along the DNA fiber. Indeed, topoisomerase inactivation leads to interesting effects on meiotic DSB timing, causing delays in *top1* mutants and accelerated DSB induction in *top2-1* mutants. The opposing effects may reflect preferences in the resolution of positive and negative supercoils between the two topoisomerases (Fernandez et al, 2014; French et al, 2011), which would imply a function for DNA topology in the timing of DSB formation. However, it is equally possible that the delayed DSB formation in *top1* mutants arises indirectly from transcriptional defects that delay expression of DSB factors. In addition, depletion of Top2 did not accelerate DSB formation, suggesting that the acceleration in *top2-1* mutants is linked to the persistence of inactive Top2 on chromatin.

The finding that *top2-1* does not disappear from chromosomes upon temperature shift (34°C) was unexpected given the widespread use of this allele. Biochemical studies showed that enzymatic activity is essentially undetectable in this mutant at 30°C (DiNardo et al, 1984). These findings indicate that *top2-1* produces a catalytically impaired enzyme that retains the capacity to associate with meiotic chromosomes, albeit with somewhat altered distribution. Given that neither the early DSB phenotype, nor the delayed chromosome remodeling is observed upon Top2 depletion, it is likely that these phenotypes depend on the presence of the inactive enzyme. It is possible that binding of the inactive enzyme hinders access of other factors that could substitute for Top2 function (e.g. Top1). Alternatively, Top2 may no longer be recruited to sites of

topological stress, with the remaining binding depending on interactions with other protein components of meiotic chromosomes, such as Hop1. In this case, the observed phenotypes could be the result of impaired meiotic chromosome dynamics rather than a buildup of topological stress. Top2 physically interacts with the recombinase Dmc1 in *Corpinus cinereus* (Iwabata et al, 2005), and recent analyses of yeast Top2 in the context of meiotic DNA repair also showed differences between mutants failing to express Top2 and mutants expressing a catalytic-dead enzyme (Zhang et al, 2014). Thus, the meiotic roles of Top2 may not be limited to its catalytic activity.

Our analyses suggest that the delay in DSB repair in *top2-1* mutants may in part be linked to impaired meiotic chromosome morphogenesis. In wild-type meiosis, assembly of the SC coincides with removal of the HORMAD factor Hop1 from chromosomes, leading to a down-regulation of new DSB formation and an easing of meiosis-specific repair restrictions (Subramanian et al, 2016; Thacker et al, 2014). By contrast, meiotic chromosomes of *top2-1* mutants accumulate SC structures that remain decorated with Hop1, as well as “train-track” chromosomes by DAPI analysis. Both phenotypes and the concomitant delay in meiotic DSB repair are characteristic of a failure to recruit the conserved chromosome remodeler Pch2 (Borner et al, 2008; Subramanian et al, 2016), whose recruitment is notably delayed in *top2-1* mutants. These data indicate that Top2 functions upstream of Pch2 in promoting the remodeling meiotic chromosomes during meiotic chromosome synapsis. They also indicate that even though Pch2 binding requires Zip1 deposition (San-Segundo & Roeder, 1999), Pch2 is not simply recruited by the assembly of the SC. Rather, these data point to a structural transition following SC deposition that needs to occur to promote Pch2 binding. On wild-type chromosomes, this transition is likely tightly coupled to SC deposition, leading to minimal overlap between Hop1-decorated axes and the SC and only transient appearance of DAPI “train-tracks”.

The separation between SC deposition and structural remodeling of the SC in *top2-1* mutant is reminiscent of meiotic chromosome morphogenesis in *Caenorhabditis elegans* (Libuda et al, 2013; Pattabiraman et al, 2017). Our results suggest that Top2 plays a role in this transition.

Topoisomerase inactivity appears to perturb multiple events during meiotic recombination. We speculate that this pleiotropic dependence is related to the cycles of expansion and compression of the chromatin fiber volume throughout prophase (Kleckner et al, 2004). These fluctuations are accompanied by stresses on the chromosomes, including twisting and buckling, which are likely used to promote progression through meiotic prophase by signaling or driving changes (Kleckner et al, 2004). Intriguingly, the three major cycles of expansion and compression are predicted to correspond to DNA breakage, axial transitions, and untangling of chromatids, which coincides well with the *top2*-associated phenotypes observed by others and us (Rose & Holm, 1993). Thus, Top2 may affect the timing of meiotic prophase by contributing to the volume fluctuation of meiotic chromosomes.

Materials and Methods

Yeast strains and growth conditions

All strains used in this study were of the SK1 background, with the exception of the SK288c spike-in strain used for SNP-ChIP analysis (Vale-Silva et al, 2019) and the *top2-1* mutant, which is congenic to SK1 (backcrossed >7x). The genotypes are listed in **Table S1**. Sequencing of the *top2-1* mutant revealed a single non-synonymous amino acid change: G829D. To induce synchronous meiosis, strains were inoculated at OD600 = 0.3 in BYTA medium for 16.5 hours at 30°C. Cultures were washed twice with water and resuspended into SPO medium at OD600 = 1.9−2.0 at 30°C as described (Blitzblau & Hochwagen, 2013). *top2-1* cells were inoculated at OD600 = 0.8 in BYTA medium for 20 hours at room temperature. For experiments that included *top2-1* mutants, SPO cultures for all strains were washed twice with water and resuspended into SPO medium at OD600 = 1.9 at room temperature and shifted to 34°C after 1 hour.

Chromatin immunoprecipitation

At the indicated time points, 25 ml of meiotic culture was harvested and fixed for 30 min in 1% formaldehyde. Formaldehyde was quenched by addition of 125 mM glycine and samples processed as described (Blitzblau & Hochwagen, 2013). Samples were immunoprecipitated with 2 µL of either anti-Top2 (TopoGEN, #TG2014), anti-MYC 9E11 (Abcam, #ab56), or anti-Red1 (kind gift of N. Hollingsworth, #16440) per IP. For SNP-ChIP experiments, previously fixed and aliquoted SK288c cells were mixed with each sample to 20% of total cell number prior to sample processing for ChIP (Vale-Silva et al, 2019). Library preparation was completed as described (Sun et al, 2015). Library quality was confirmed by Qubit HS assay kit and 2200 TapeStation. 51bp, 75bp, or 100bp single-end sequencing was accomplished on an Illumina HiSeq 2500 or NextSeq 500 instrument. Read length and sequencing instrument did not seem to introduce any

biases to the results.

Mononucleosomal DNA preparation

At the 3-hr time point, 50 ml of meiotic culture was harvested and fixed for 30 min in 1% formaldehyde. The formaldehyde was quenched by addition of 125 mM glycine and samples processed as described (Pan et al, 2011). Library preparation and sequencing were done identically to methods for chromatin immunoprecipitation above.

Processing of Illumina sequence data

Sequencing reads were mapped to the SK1 genome (Yue et al, 2017) using Bowtie. Sequencing reads of 75bp or 100bp were clipped to 51bp. For paired-end sequencing, only single-end information was used. Only perfect matches across all 51bp were considered during mapping. Multiple alignments were not taken into account, which means each read only mapped to one location in the genome. Reads were extended towards 3' ends to a final length of 200bp and probabilistically determined PCR duplications were removed in MACS-2.1.1 (https://github.com/taoliu/MACS) (Zhang et al, 2008). For data processing of mononucleosomal reads using Bowtie, bandwidth (--bw) was set to 350 for model building in MACS2, and reads were extended towards 3' ends to a final length of 146bp. All pileups were SPMR-normalized (signal per million reads), and for ChIP-seq data, fold-enrichment of the ChIP data over the input data was calculated. Plots shown were made using two combined replicates. Mononucleosomal DNA data was combined with previously published data from (Pan et al, 2011).

Peak Calling

To identify Top1 and Top2 protein enriched regions (peaks) for **Figure 4e**, MACS-2.1.1 (https://github.com/taoliu/MACS) (Zhang et al, 2008) was used for peak calling of the

sequence data by extending reads towards 3' ends to a final length of 200bp, removing probabilistically determined PCR duplicates and using the --broad flag to composite nearby highly enriched regions that meet the default q-value cutoff.

mRNA preparation and sequencing

At the 3-hr time point, 1.5 ml of meiotic culture was harvested. The cells were washed in TE buffer and lysed by mechanical disruption with glass beads at 4°C. The lysate supernatant was mixed with an equivalent volume of freshly prepared 70% ethanol and purified using the RNeasy RNA isolation Kit (Qiagen). mRNA was extracted from approximately 5 µg of the total RNA samples using Sera-Mag oligo-dT beads (GE Healthcare Life Sciences). The mRNA was fragmented and used to prepare sequencing libraries according to the Illumina TruSeq Stranded mRNA sample preparation kit. Briefly, the prepared mRNA was used as a template to synthesize first-strand cDNA. Second-strand cDNA was synthesized from the first strand with the incorporation of deoxyuridine triphosphates. Finally, sequencing libraries were prepared by PCR from the cDNA samples after ligation of adapters and sequenced on an Illumina HiSeq-2500 instrument with a read length of 51 nucleotides and single-end configuration.

RNA-seq data analysis

Single-end stranded reads were mapped to the SK1 genome assembly (Yue et al, 2017) using Tophat2 (version 2.1.1; Bowtie version 2.2.9) with first-strand library type, no novel junctions, and otherwise default options (Kim et al, 2013). Mapped reads were counted using featureCounts (from subread version 1.5.1) with default options (Liao et al, 2014). Statistical analysis was performed using a count-based workflow (Anders et al, 2013) with the edgeR Bioconductor package (version 3.12.1; (Robinson et al, 2010)). Briefly, gene counts were normalized to counts per million (cpm) reads and genes with less than

10-15 mapped reads were filtered out. Transcriptome composition bias between samples was eliminated using edgeR's default trimmed mean of M-values (TMM) normalization. Gene length-corrected counts were calculated as transcripts per million (tpm; (Wagner et al, 2012)) and differential expression analyses were performed using the generalized linear model (GLM) quasi-likelihood (QL) F-test in edgeR. Multiplicity correction is performed with the Benjamini-Hochberg method on the p-values to control the false discovery rate (FDR).

Mapping Spo11 oligos to SK1 genome

The Spo11-oligo raw reads were downloaded from GEO and, after combining replicates, the adaptors were clipped with fastx_clipper (fastx_toolkit/intel/0.0.14) using the following parameters: -a AGATCGGAAGAGCACACGTCTGAACTCCAGTCAC -l 15 -n -v -Q33. Reads were then trimmed using fastq_quality_trimmer with a minimum quality threshold of 20 and a minimum length of 20. The trimmed reads were mapped to the SK1 genome using BWA (bwa/intel/0.7.15), extended to 37bp, and SPMR-normalized. Peaks were identified by MACS2 using the default q-value cutoff while bypassing the shifting model. Peaks below the median signal value were discarded.

Chromosome spreads

Meiotic nuclear spreads were performed as described (Subramanian et al, 2016). Top2 was detected using anti-Top2 (TopoGEN, #TG2014) rabbit serum at 1:200 in blocking buffer and Alexa Fluor 488 anti-rabbit (Jackson ImmunoResearch) at 1:200. Zip1 was detected using Zip1 yC-19 goat antibody (Santa Cruz Biotechnology) at 1:200 and anti-goat Cy3 at 1:200 (Jackson ImmunoResearch). Top1 was detected using anti-Myc mouse serum (Millipore 4A6) at 1:100 and FITC anti-mouse (Jackson ImmunoResearch) at 1:200. Hop1 was detected using anti-Hop1 rabbit serum (kind gift of N. Hollingsworth)

at 1:200 and Alexa Fluor 488 anti-rabbit at 1:200. Pch2 was detected using anti-Pch2 (kind gift of A. Shinohara) at 1:200 and Alexa Fluor 488 anti-rabbit at 1:200. Microscopy and image processing were carried out using a Deltavision Elite imaging system (Applied Precision) adapted to an Olympus IX17 microscope and analyzed using softWoRx 5.0 software.

Southern analysis

For pulsed-field gel analysis and analysis of individual DSB hotspots by standard electrophoresis, genomic DNA was purified in agarose plugs as described (Subramanian et al, 2019). DNA was digested in-gel for analysis of DSB hotspots. Samples were melted at 65°C prior to loading. Pulse-field gel electrophoresis and Southern blotting of chromosome VIII using the *CBP2* probe was performed as described (Blitzblau et al, 2007). Analysis of the *CCT6* hotspot used a HindIII digest and a previously described probe (Thacker et al, 2014). Analysis of the *CPA2* hotspot used an XhoI digest and a probe spanning ChrX: 640,208-641,235 in the sacCer3 reference genome. Hybridization signal was detected using a Typhoon FLA 9000.

Acknowledgements

We thank A. Amon and S. Biggins for sharing strains, N. Hollingsworth and A. Shinohara for sharing antibodies, S. Keeney for helpful discussions, and the NYU Department of Biology Sequencing Core for technical assistance and data processing. This work was supported by the National Institutes of Health [GM123035 to AH].

Author contributions

Conceptualization, J.H., X.S. and A.H.; Investigation, J.H., X.S., L.A.V.S., T.E.M., and A.H.; Software, J.H.; Formal Analysis, J.H. and A.H.; Resources, J.H., X.S. and A.H.; Writing – Original Draft, J.H and A.H.; Writing – Review & Editing, J.H., X.S., L.A.V.S., T.E.M., and A.H.

Conflict of Interest

The authors declare no conflict of interest.

Data Availability

The datasets and computer code produced in this study are available in following databases:

- RNA-seq data, ChIP-seq data, and SNP-ChIP data: Gene Expression Omnibus GSE131994 'https://www.ncbi.nlm.nih.gov/geo/query/acc.cgi?acc=GSE131994'
- Computer scripts for processing Illumina reads: Github 'https://github.com/hochwagenlab/ChIPseq_functions/tree/master/ChIPseq_Pipeline_v3/'
- Computer scripts for processing SNP-ChIP reads and calculating spike-in normalization factor: Github

'https://github.com/hochwagenlab/ChIPseq_functions/tree/master/ChIPseq_Pipeline_hybrid_genome/ '

References

Anders S, McCarthy DJ, Chen Y, Okoniewski M, Smyth GK, Huber W, Robinson MD (2013) Count-based differential expression analysis of RNA sequencing data using R and Bioconductor. *Nat Protoc* **8:** 1765-1786

Baudat F, Nicolas A (1997) Clustering of meiotic double-strand breaks on yeast chromosome III. *Proc Natl Acad Sci U S A* **94:** 5213-5218

Bermejo R, Doksani Y, Capra T, Katou YM, Tanaka H, Shirahige K, Foiani M (2007) Top1- and Top2-mediated topological transitions at replication forks ensure fork progression and stability and prevent DNA damage checkpoint activation. *Genes Dev* **21:** 1921-1936

Bishop DK, Park D, Xu L, Kleckner N (1992) DMC1: a meiosis-specific yeast homolog of E. coli recA required for recombination, synaptonemal complex formation, and cell cycle progression. *Cell* **69:** 439-456

Blitzblau HG, Bell GW, Rodriguez J, Bell SP, Hochwagen A (2007) Mapping of meiotic single-stranded DNA reveals double-stranded-break hotspots near centromeres and telomeres. *Curr Biol* **17:** 2003-2012

Blitzblau HG, Hochwagen A (2013) ATR/Mec1 prevents lethal meiotic recombination initiation on partially replicated chromosomes in budding yeast. *Elife* **2:** e00844

Borde V, de Massy B (2013) Programmed induction of DNA double strand breaks during meiosis: setting up communication between DNA and the chromosome structure. *Curr Opin Genet Dev* **23:** 147-155

Borde V, Wu TC, Lichten M (1999) Use of a recombination reporter insert to define meiotic recombination domains on chromosome III of Saccharomyces cerevisiae. *Mol Cell Biol* **19:** 4832-4842

Borner GV, Barot A, Kleckner N (2008) Yeast Pch2 promotes domainal axis organization, timely recombination progression, and arrest of defective recombinosomes during meiosis. *Proc Natl Acad Sci U S A* **105:** 3327-3332

Cheng CH, Lo YH, Liang SS, Ti SC, Lin FM, Yeh CH, Huang HY, Wang TF (2006) SUMO modifications control assembly of synaptonemal complex and polycomplex in meiosis of Saccharomyces cerevisiae. *Genes Dev* **20:** 2067-2081

Cheng Z, Otto GM, Powers EN, Keskin A, Mertins P, Carr SA, Jovanovic M, Brar GA (2018) Pervasive, Coordinated Protein-Level Changes Driven by Transcript Isoform Switching during Meiosis. *Cell* **172:** 910-923 e916

Christman MF, Dietrich FS, Fink GR (1988) Mitotic recombination in the rDNA of S. cerevisiae is suppressed by the combined action of DNA topoisomerases I and II. *Cell* **55:** 413-425

Cobb J, Miyaike M, Kikuchi A, Handel MA (1999) Meiotic events at the centromeric heterochromatin: histone H3 phosphorylation, topoisomerase II alpha localization and chromosome condensation. *Chromosoma* **108:** 412-425

Cobb J, Reddy RK, Park C, Handel MA (1997) Analysis of expression and function of topoisomerase I and II during meiosis in male mice. *Mol Reprod Dev* **46:** 489-498

Cohen BA, Mitra RD, Hughes JD, Church GM (2000) A computational analysis of whole-genome expression data reveals chromosomal domains of gene expression. *Nat Genet* **26:** 183-186

DiNardo S, Voelkel K, Sternglanz R (1984) DNA topoisomerase II mutant of Saccharomyces cerevisiae: topoisomerase II is required for segregation of daughter molecules at the termination of DNA replication. *Proc Natl Acad Sci U S A* **81:** 2616-2620

Fernandez X, Diaz-Ingelmo O, Martinez-Garcia B, Roca J (2014) Chromatin regulates DNA torsional energy via topoisomerase II-mediated relaxation of positive supercoils. *EMBO J* **33:** 1492-1501

French SL, Sikes ML, Hontz RD, Osheim YN, Lambert TE, El Hage A, Smith MM, Tollervey D, Smith JS, Beyer AL (2011) Distinguishing the roles of Topoisomerases I and II in relief of transcription-induced torsional stress in yeast rRNA genes. *Mol Cell Biol* **31:** 482-494

Gittens W, Johnson DJ, Allison RM, Cooper TJ, Thomas H, Neale MJ (2019) A nucleotide resolution map of Top2-linked DNA breaks in the yeast and human genome. *bioRxiv***:** 530667

Gomez R, Viera A, Berenguer I, Llano E, Pendas AM, Barbero JL, Kikuchi A, Suja JA (2014) Cohesin removal precedes topoisomerase IIalpha-dependent decatenation at centromeres in male mammalian meiosis II. *Chromosoma* **123:** 129-146

Handel MA, Caldwell KA, Wiltshire T (1995) Culture of pachytene spermatocytes for analysis of meiosis. *Dev Genet* **16:** 128-139

Hartsuiker E, Bahler J, Kohli J (1998) The role of topoisomerase II in meiotic chromosome condensation and segregation in Schizosaccharomyces pombe. *Mol Biol Cell* **9:** 2739-2750

Haruki H, Nishikawa J, Laemmli UK (2008) The anchor-away technique: rapid, conditional establishment of yeast mutant phenotypes. *Mol Cell* **31:** 925-932

Hassold T, Sherman S (2000) Down syndrome: genetic recombination and the origin of the extra chromosome 21. *Clin Genet* **57:** 95-100

Hughes SE, Hawley RS (2014) Topoisomerase II is required for the proper separation of heterochromatic regions during Drosophila melanogaster female meiosis. *PLoS Genet* **10:** e1004650

Iwabata K, Koshiyama A, Yamaguchi T, Sugawara H, Hamada FN, Namekawa SH, Ishii S, Ishizaki T, Chiku H, Nara T, Sakaguchi K (2005) DNA topoisomerase II interacts with Lim15/Dmc1 in meiosis. *Nucleic Acids Res* **33:** 5809-5818

Jaramillo-Lambert A, Fabritius AS, Hansen TJ, Smith HE, Golden A (2016) The Identification of a Novel Mutant Allele of topoisomerase II in Caenorhabditis elegans Reveals a Unique Role in Chromosome Segregation During Spermatogenesis. *Genetics* **204:** 1407-1422

Kallio M, Lahdetie J (1996) Fragmentation of centromeric DNA and prevention of homologous chromosome separation in male mouse meiosis in vivo by the topoisomerase II inhibitor etoposide. *Mutagenesis* **11:** 435-443

Kim D, Pertea G, Trapnell C, Pimentel H, Kelley R, Salzberg SL (2013) TopHat2: accurate alignment of transcriptomes in the presence of insertions, deletions and gene fusions. *Genome Biol* **14:** R36

Kleckner N, Zickler D, Jones GH, Dekker J, Padmore R, Henle J, Hutchinson J (2004) A mechanical basis for chromosome function. *Proc Natl Acad Sci U S A* **101:** 12592-12597

Klein F, Laroche T, Cardenas ME, Hofmann JF, Schweizer D, Gasser SM (1992) Localization of RAP1 and topoisomerase II in nuclei and meiotic chromosomes of yeast. *J Cell Biol* **117:** 935-948

Lam I, Keeney S (2015a) Mechanism and regulation of meiotic recombination initiation. *Cold Spring Harb Perspect Biol* **7:** a016634

Lam I, Keeney S (2015b) Nonparadoxical evolutionary stability of the recombination initiation landscape in yeast. *Science* **350:** 932-937

Liao Y, Smyth GK, Shi W (2014) featureCounts: an efficient general purpose program for assigning sequence reads to genomic features. *Bioinformatics* **30:** 923-930

Libuda DE, Uzawa S, Meyer BJ, Villeneuve AM (2013) Meiotic chromosome structures constrain and respond to designation of crossover sites. *Nature* **502:** 703-706

Martinez-Garcia M, Schubert V, Osman K, Darbyshire A, Sanchez-Moran E, Franklin FCH (2018) TOPII and chromosome movement help remove interlocks between entangled chromosomes during meiosis. *J Cell Biol* **217:** 4070-4079

Mengoli V, Bucciarelli E, Lattao R, Piergentili R, Gatti M, Bonaccorsi S (2014) The analysis of mutant alleles of different strength reveals multiple functions of topoisomerase 2 in regulation of Drosophila chromosome structure. *PLoS Genet* **10:** e1004739

Moens PB, Earnshaw WC (1989) Anti-topoisomerase II recognizes meiotic chromosome cores. *Chromosoma* **98:** 317-322

Pan J, Sasaki M, Kniewel R, Murakami H, Blitzblau HG, Tischfield SE, Zhu X, Neale MJ, Jasin M, Socci ND, Hochwagen A, Keeney S (2011) A hierarchical combination of

factors shapes the genome-wide topography of yeast meiotic recombination initiation. *Cell* **144:** 719-731

Pattabiraman D, Roelens B, Woglar A, Villeneuve AM (2017) Meiotic recombination modulates the structure and dynamics of the synaptonemal complex during C. elegans meiosis. *PLoS Genet* **13:** e1006670

Petronczki M, Siomos MF, Nasmyth K (2003) Un menage a quatre: the molecular biology of chromosome segregation in meiosis. *Cell* **112:** 423-440

Pommier Y, Sun Y, Huang SN, Nitiss JL (2016) Roles of eukaryotic topoisomerases in transcription, replication and genomic stability. *Nat Rev Mol Cell Biol* **17:** 703-721

Robinson MD, McCarthy DJ, Smyth GK (2010) edgeR: a Bioconductor package for differential expression analysis of digital gene expression data. *Bioinformatics* **26:** 139-140

Rose D, Holm C (1993) Meiosis-specific arrest revealed in DNA topoisomerase II mutants. *Mol Cell Biol* **13:** 3445-3455

Rose D, Thomas W, Holm C (1990) Segregation of recombined chromosomes in meiosis I requires DNA topoisomerase II. *Cell* **60:** 1009-1017

Russell LB, Hunsicker PR, Hack AM, Ashley T (2000) Effect of the topoisomerase-II inhibitor etoposide on meiotic recombination in male mice. *Mutat Res* **464:** 201-212

Rutledge MT, Russo M, Belton JM, Dekker J, Broach JR (2015) The yeast genome undergoes significant topological reorganization in quiescence. *Nucleic Acids Res* **43:** 8299-8313

San-Segundo PA, Roeder GS (1999) Pch2 links chromatin silencing to meiotic checkpoint control. *Cell* **97:** 313-324

Smith AV, Roeder GS (1997) The yeast Red1 protein localizes to the cores of meiotic chromosomes. *J Cell Biol* **136:** 957-967

Sperling AS, Jeong KS, Kitada T, Grunstein M (2011) Topoisomerase II binds nucleosome-free DNA and acts redundantly with topoisomerase I to enhance recruitment of RNA Pol II in budding yeast. *Proc Natl Acad Sci U S A* **108:** 12693-12698

Stern H, Hotta Y (1983) Meiotic aspects of chromosome organization. *Staedler Symp* **15:** 25-41

Subramanian VV, MacQueen AJ, Vader G, Shinohara M, Sanchez A, Borde V, Shinohara A, Hochwagen A (2016) Chromosome Synapsis Alleviates Mek1-Dependent Suppression of Meiotic DNA Repair. *PLoS Biol* **14:** e1002369

Subramanian VV, Zhu X, Markowitz TE, Vale-Silva LA, San-Segundo PA, Hollingsworth NM, Keeney S, Hochwagen A (2019) Persistent DNA-break potential near telomeres increases initiation of meiotic recombination on short chromosomes. *Nat Commun* **10:** 970

Sun X, Huang L, Markowitz TE, Blitzblau HG, Chen D, Klein F, Hochwagen A (2015) Transcription dynamically patterns the meiotic chromosome-axis interface. *Elife* **4:** e07424

Swygert SG, Kim S, Wu X, Fu T, Hsieh TH, Rando OJ, Eisenman RN, Shendure J, McKnight JN, Tsukiyama T (2019) Condensin-Dependent Chromatin Compaction Represses Transcription Globally during Quiescence. *Mol Cell* **73:** 533-546 e534

Tateno H, Kamiguchi Y (2001) Meiotic stage-dependent induction of chromosome aberrations in Chinese hamster primary oocytes exposed to topoisomerase II inhibitor etoposide. *Mutat Res* **476:** 139-148

Teves SS, Henikoff S (2014) Transcription-generated torsional stress destabilizes nucleosomes. *Nat Struct Mol Biol* **21:** 88-94

Thacker D, Mohibullah N, Zhu X, Keeney S (2014) Homologue engagement controls meiotic DNA break number and distribution. *Nature* **510:** 241-246

Vale-Silva LA, Markowitz TE, Hochwagen A (2019) SNP-ChIP: a versatile and tag-free method to quantify changes in protein binding across the genome. *BMC Genomics* **20:** 54

Vos SM, Tretter EM, Schmidt BH, Berger JM (2011) All tangled up: how cells direct, manage and exploit topoisomerase function. *Nat Rev Mol Cell Biol* **12:** 827-841

Wagner GP, Kin K, Lynch VJ (2012) Measurement of mRNA abundance using RNA-seq data: RPKM measure is inconsistent among samples. *Theory Biosci* **131:** 281-285

Wang JC (2002) Cellular roles of DNA topoisomerases: a molecular perspective. *Nat Rev Mol Cell Biol* **3:** 430-440

Yu HG, Koshland DE (2003) Meiotic condensin is required for proper chromosome compaction, SC assembly, and resolution of recombination-dependent chromosome linkages. *J Cell Biol* **163:** 937-947

Yue JX, Li J, Aigrain L, Hallin J, Persson K, Oliver K, Bergstrom A, Coupland P, Warringer J, Lagomarsino MC, Fischer G, Durbin R, Liti G (2017) Contrasting evolutionary genome dynamics between domesticated and wild yeasts. *Nat Genet* **49:** 913-924

Zhang L, Wang S, Yin S, Hong S, Kim KP, Kleckner N (2014) Topoisomerase II mediates meiotic crossover interference. *Nature* **511:** 551-556

Zhang Y, Liu T, Meyer CA, Eeckhoute J, Johnson DS, Bernstein BE, Nusbaum C, Myers RM, Brown M, Li W, Liu XS (2008) Model-based analysis of ChIP-Seq (MACS). *Genome Biol* **9:** R137

Zickler D, Kleckner N (2015) Recombination, Pairing, and Synapsis of Homologs during Meiosis. *Cold Spring Harb Perspect Biol* **7:** a016626

Figure Legends

Figure 1. Topoisomerases are enriched in promoter-containing IGRs.

(a) Wild type genomic distribution of Top1-13myc and Top2 on a section chromosome II at the time of meiotic DSB formation (3h after meiotic induction) as measured by ChIP-seq. **(b)** Metagene analysis Top1 and Top2 enrichment. Start and end positions of the scaled open reading frame (ORF) are indicated. **(c)** Top2 enrichment centered at the midpoints of IGRs parsed into divergent, tandem, and convergent regions. The 95% confidence interval is shown for average lines in (b,c). Heat maps of **(d)** Top1 and **(e)** Top2 localization centered at midpoints of all IGRs containing promoters (i.e. divergent and tandem), sorted by size of the IGR. Black lines delineate start or end of ORFs bordering the IGR. Average **(f)** Top1 and **(g)** Top2 signal in quartiles based on IGR size. Quartile ranges are <294 bp (purple), 294 - 453 bp (green), 454 - 752 bp (red), and >752 bp (black). Signals are centered at IGR midpoints and extended 1kb in each direction. The standard error for the average lines are shown for (f,g).

Figure 2. Transcriptional activity during meiotic prophase.

(a) Top1 and **(b)** Top2 localization in the vicinity of starts and ends of ORFs, sorted based on transcriptional activity of the associated gene. The average of each quantile is plotted above the heat maps. The color of the lines corresponds to the color segments beside the 4 quartiles of transcriptional activity. The standard error for the average quantile lines are shown. Box plots showing the size distribution of **(c)** divergent and tandem IGRs during meiosis for gene pairs with either extremely high or low levels of transcriptional activity. The number of gene pairs is noted above the respective box. Significance was determined by unpaired, two-sided Wilcoxon test. **(d)** Similar analysis as in (c) for divergent IGRs in vegetative and pre-meiotic cells using data from (Cheng et

al, 2018). Note that gene pair identity changes as a function of the transcriptional program in the different developmental stages. ***$P < 0.001$ and n.s. P-value=0.71 (c) and P-value=0.54 (d), Mann-Whitney-Wilcoxon test.

Figure 3. Top2 abundance on chromosomes increases during meiosis.

(a) Comparison of the level of total chromosomal association of Top2 on pre-meiotic (0h) and meiotic chromosomes (3h after meiotic induction) as determined by SNP-ChIP analysis. Points represent individual replicate values and bars represent average. Values are normalized to the pre-meiotic levels for each experimental replicate. **(b-c)** Top2 binding in promoters parsed by size of the promoter-containing IGR on **(b)** pre-meiotic or **(c)** meiotic chromosomes using quantitative SNP-ChIP normalization. Quantile ranges are <338 bp (blue), 338-625 bp (green), and >625 bp (red). **(d-f)** Spike-in adjusted comparison of Top2 binding on pre-meiotic and meiotic chromosomes centered at **(d)** convergent IGRs, **(e)** promoter-containing IGRs, and **(f)** DSB hotspots. The 95% confidence interval is shown for average lines in (b-f).

Figure 4. Topoisomerase recruitment to meiotic chromosomes.

(a) Spo11-oligo signal in promoters and at gene ends plotted as heat maps. Signal tracks are sorted based on transcriptional activity of the associated gene. Colored triangle segments indicate 4 quartiles of transcriptional activity. The average of each quantile is plotted above the heat maps. Heat maps of **(b)** Spo11 oligo signal and **(c)** nucleosome signal determined by MNase-seq across all promoter regions sorted by IGR size. Black lines delineate IGR borders. **(d)** Top1-myc and Top2 binding centered at hotspot summits. Heat maps show all hotspots sorted by level of breakage activity. Average of each quantile is plotted above the heat maps, with the color of the line corresponding to the color beside the heat map quantile. The standard error for the

average quantile lines are shown for (a,d). **(e)** Comparison of hotspot activity based on colocalization of a hotspot with a significant peak of either “no topoisomerase”, “Top1”, “Top2”, or “both Top1 and Top2”. Number of hotspots in each group is labeled above the respective box in the plot. ***P < 0.0001, **P < 0. 01, Mann-Whitney-Wilcoxon test with Bonferroni correction.

Figure 5. Effects of topoisomerases on DSB activity.

(a) DNA content of wild type and *top1Δ* cells as determined by flow cytometry. Samples were taken at the indicated time points. **(b)** PFGE/Southern analysis of DSBs along chromosome VIII in *dmc1Δ* and *dmc1Δ top1Δ* cells. **(c)** Quantification of DSB signal in (b) calculated as fraction of total signal (parental and DSB) after background subtraction. **(d-f)** Time course analysis of *dmc1Δ* and *dmc1Δ top2-1* cells shifted from room temperature to the restrictive temperature (34°C) 1h after meiotic induction. The analyses methods are the same as in (a-c).

Figure 6. Delayed DSB repair due to inactive Top2 on chromosomes.

(a) Southern blot analysis of DSBs throughout a meiotic time course across chromosome VIII in wild type and *top2-1* cells. Cultures were shifted to the restrictive temperature (34°C) 1h after meiotic induction. **(b)** Immunofluorescence staining for Top2, Zip1, and DAPI on chromosome spreads of wild type and the *top2-1* mutant at the restrictive temperature. Scale bars are 5 μm. **(c)** Metagene analysis of Top2 in wild type and the *top2-1* mutant at the restrictive temperature. The 95% confidence interval is shown for the average signals. **(d)** Representative distribution at 34°C of Top2 (in wild type and the *top2-1* mutant) and the chromosome axis protein Red1 (in wild type) compared to Spo11 cleavage patterns along a region of chromosome XII. **(e)** Immunofluorescence staining for Top2 and Zip1 on chromosome spreads of *Top2-FRB*

cells without and with the addition of rapamycin to deplete Top2-FRB from the nucleus. Scale bars are 5 µm. **(f)** Southern blot analysis of the no tag control compared to *Top2-FRB* without and with the addition of rapamycin across chromosome VIII. Roman numerals mark the hotspot signals quantified in **Fig S4C**.

Figure 7. Inactive Top2 delays meiotic chromosome transitions.

(a) Immunofluorescence staining for Hop1 and Zip1 on chromosome spreads of wild type and the *top2-1* mutant during meiosis at 34°C, as well as *TOP2-FRB* without and with the addition of rapamycin (30°C). Scale bars are 5 µm. **(b)** Quantification of chromosomal phenotypes as determined by DAPI staining of chromosome spreads containing tracks of Zip1 marking late prophase. Images show representative examples of chromosomal phenotypes. Analysis is shown for wild type, *top2-1, TOP2-FRB,* and *TOP2-FRB* with the addition of rapamycin. The number of nuclei counted are indicated above the respective bar in the plot. **(c)** Immunofluorescence staining for Pch2 and Zip1 on wild type and the *top2-1* chromosome spreads throughout a meiotic time course at 34°C. Scale bars are 5 µm.

Supplemental Material

Supplemental Figure 1. Topoisomerases are abundant on chromosomes throughout meiotic prophase.

(a-b) Immunofluorescence staining of chromosome spreads throughout meiotic prophase. **(a)** Top1-myc nuclei and wild type no-tag control nuclei stained for Myc, Zip1, and DAPI. White arrowhead marks the nucleolus. Scale bars are 5 μm. **(b)** Wild type nuclei stained for Top2, Zip1, and DAPI. Scale bars are 5μm. **(c)** Top1-myc localization centered at the midpoints of IGRs, parsed into divergent, tandem, and convergent regions. The 95% confidence interval is shown for average lines.

Supplemental Figure 2. Transcription is most active in genes sharing wide divergent promoter regions during starvation.

Box plots of size of divergent regions for highly and lowly transcribed gene pairs during meiosis at 3h and 10h and in non-meiotic *MATa/a* cells in sporulation media (Cheng et al, 2018). The number of gene pairs is noted above the respective box.

***P < 0.00001, **P < 0. 01, Mann-Whitney-Wilcoxon test.

Supplemental Figure 3. DSB initiation is accelerated in *top2-1*.

Southern blot analysis of the **(a)** *CCT6* and **(b)** *CPA2* hotspots throughout a meiotic time course in *dmc1Δ* and *dmc1Δ top2-1* cells. Cells were shifted to 34°C 1h after meiotic induction. **(c)** Southern blot analysis of DSBs throughout a meiotic time course across chromosome VIII in *dmc1Δ*, *dmc1Δ spo11Δ*, and *dmc1Δ spo11Δ top2-1* cells. Both panels are taken from the same Southern blot image.

Supplemental Figure 4. Top2 promotes DSB repair.

(a) Southern blot analysis of DSBs throughout a meiotic time course across chromosome VIII in wild type and *top1Δ* cells. Both panels are taken from the same Southern blot. **(b)** DNA content of *TOP2-FRB* strains without and with the addition of rapamycin as determined by flow cytometry. **(c)** Quantification of DSBs from **Fig 6f** and replicate Southern blot (not shown), normalized by subtracting background, dividing by total DNA content, and finally dividing strain plus rapamycin by strain minus rapamycin. **(d)** Southern blot analysis of the *CCT6* hotspot in the no-tag control and *TOP2-FRB* without and with the addition of rapamycin in a *dmc1Δ* background. **(e)** Quantification of the *CCT6* hotspot Southern blot band throughout the meiotic time course.

Supplemental Table 1. Strains used in this study

Strain	Genotype	Background	Used in Figure Panel	Reference
H119	*MATa, ho::LYS2, lys2, ura3, leu2::hisG, his4B::LEU2, arg4-Bgl II* *MATalpha, ho::LYS2, lys2, ura3, leu2::hisG, his4X::LEU2 (Bam)-URA3, arg4-Nsp*	SK1	2, 4a, 6a-b, 7a-b, S2	(Bishop et al, 1992)
H7797	*MATa, ho::LYS2, lys2, ura3, leu2::hisG, his3::hisG, trp1::hisG* *MATalpha, ho::LYS2, lys2, URA3, LEU2, HIS3, TRP1*	SK1	1a-c, 1e, 1g, 2b, 3, 4c-e, 6c-d, 7c, S1b, S4a	(Subramanian et al, 2016)
H118	*MATa, ho::LYS2, lys2, leu2::hisG, his4X::LEU2-URA3, ura3, arg4-nsp, dmc1Δ::ARG4* *MATalpha, ho::LYS2, lys2, leu2::hisG, his4B::LEU2, ura3, arg4-Bgl2, dmc1Δ::ARG4*	SK1	5, S3c	(Bishop et al, 1992)
H7838	*MATa, ho::LYS2, lys2, ura3, leu2::hisG, his3::hisG, trp1::hisG, RPL13A-2xFKBP12::TRP1, fpr1::KanmX4, tor1-1::HIS3* *MATalpha, ho::LYS2, lys2, URA3, LEU2, his3::hisG, trp1::hisG, RPL13A-2xFKBP12::TRP1, fpr1::KanmX4, tor1-1::HIS3*	SK1	6f, S4c	(Subramanian et al, 2016)

H7602	*MATa, ho::LYS2, lys2, ura3, leu2::hisG, trp1::hisG, HIS3?,RPL13A-2xFKBP12::TRP1, fpr1::KanmX4, tor1-1::HIS3, TOP2-FRB::KanMX6* *MATalpha, ho::LYS2, lys2, URA3, leu2::hisG, trp1::hisG, HIS3?, RPL13A-2xFKBP12::TRP1, fpr1::KanmX4, tor1-1::HIS3, TOP2-FRB::KanMX6*	SK1	6e-f, 7b, S4b-c, S5	
H7606	*MATa, ho::LYS2, lys2, ura3, leu2::hisG, TRP, his4B::LEU2, arg4-Bgl II, top2-1* *MATalpha, ho::LYS2, lys2, ura3, leu2::hisG, TRP, his4X::LEU2-(Bam)-URA3, arg4-Nsp, top2-1*	SK1	6a-d, 7	
H8784	*MATalpha, ho::LYS2, lys2, ura3, leu2::hisG, TRP, his4B::LEU2, arg4-Bgl II, dmc1Δ::ARG4, top2-1* *MATa, ho::LYS2, lys2, ura3, leu2::hisG, his4X::LEU2-(Bam)-URA3, arg4-Nsp, dmc1Δ::ARG4 , top2-1*	SK1	5d-f, S3a-b	
H9847	*MATa, ho::LYS2, lys2, ura3, leu2::hisG, his3::hisG, trp1::hisG, Top1-13Myc::TRP1* *MATalpha, ho::LYS2, lys2, ura3, leu2::hisG, TRP, arg4-Nsp?, Top1-13Myc::TRP1*	SK1	1a-b, 1d, 1f, 2a, 4d, 4e, S1a, S1c	
H7652	*MATalpha, ho::LYS2, lys2, ura3, leu2::hisG, TRP, his4X::LEU2-(Bam)-URA3, arg4-Nsp, HIS3, top1Δ::KanMX6* *MATa, ho::LYS2, lys2, ura3, leu2::hisG, TRP, his4B::LEU2, arg4-Bgl II, HIS3, top1Δ::KanMX6*	SK1	S4a	
H7833	*MATa, ho::LYS2, lys2, leu2::hisG, his4X::LEU2-URA3, ura3, TRP, arg4-nsp, dmc1Δ::ARG4, top1Δ::KanMX6* *MATalpha, ho::LYS2, lys2, trp1, leu2::hisG, his4B::LEU2, ura3, arg4-Bgl2?, dmc1Δ::ARG4, top1Δ::KanMX6*	SK1	5a-c	
H9173	*MATa, ho::LYS2, lys2, ura3, leu2::hisG, TRP, his4B::LEU2, arg4-Bgl II, dmc1Δ::ARG4, spo11Δ::URA3* *MATalpha, ho::LYS2, lys2, ura3, leu2::hisG, TRP, his4B::LEU2, arg4-Bgl II, dmc1Δ::ARG4, spo11Δ::URA3*	SK1	S3c	
H9171	*MATa, ho::LYS2, lys2, ura3, leu2::hisG, TRP, his4B::LEU2, arg4-Bgl II, dmc1Δ::ARG4, top2-1, spo11Δ::URA3* *MATalpha, ho::LYS2, lys2, ura3, leu2::hisG, TRP, his4B::LEU2, arg4-Bgl II, dmc1Δ::ARG4, top2-1, spo11Δ::URA3*	SK1	S3c	

H8325	*MATalpha, ho::LYS2, lys2, ura3, leu2::hisG, his3::hisG, trp1::hisG, RPL13A-2xFKBP12::TRP1, fpr1::KanmX4, tor1-1::HIS3, dmc1□::ARG4* *MATa, ho::LYS2, lys2, ura3, leu2::hisG, his3::hisG, trp1::hisG, RPL13A-2xFKBP12::TRP1, fpr1::KanmX4, tor1-1::HIS3, dmc1□::ARG4*	SK1	S4d-e	
H8175	*MATa, ho::LYS2, lys2, ura3, leu2::hisG, TRP1?, HIS3?, arg4-Bgl2?, RPL13A-2xFKBP12::TRP1, fpr1::KanmX4, tor1-1::HIS3, TOP2-FRB::KanMX6, his4B::LEU2, dmc1□::ARG4* *MATalpha, ho::LYS2, lys2, URA3?, leu2::hisG, trp1::hisG, HIS3, arg4-nsp, RPL13A-2xFKBP12::TRP1, fpr1::KanmX4, tor1-1::HIS3, TOP2-FRB::KanMX6, his4X::LEU2-URA3, dmc1□::ARG4*	SK1	S4d-e	
H8644	*MATa, his3Δ1, LEU, LYS, ura3Δ0, RME1(ins-308a), TAO3(E1493Q), MKT1(D30G)* *MATalpha, HIS3, leu2Δ0, lys2Δ0, URA3, RME1(ins-308a), TAO3(E1493Q), MKT1(D30G)*	S288C	3	(Vale-Silva et al, 2019)

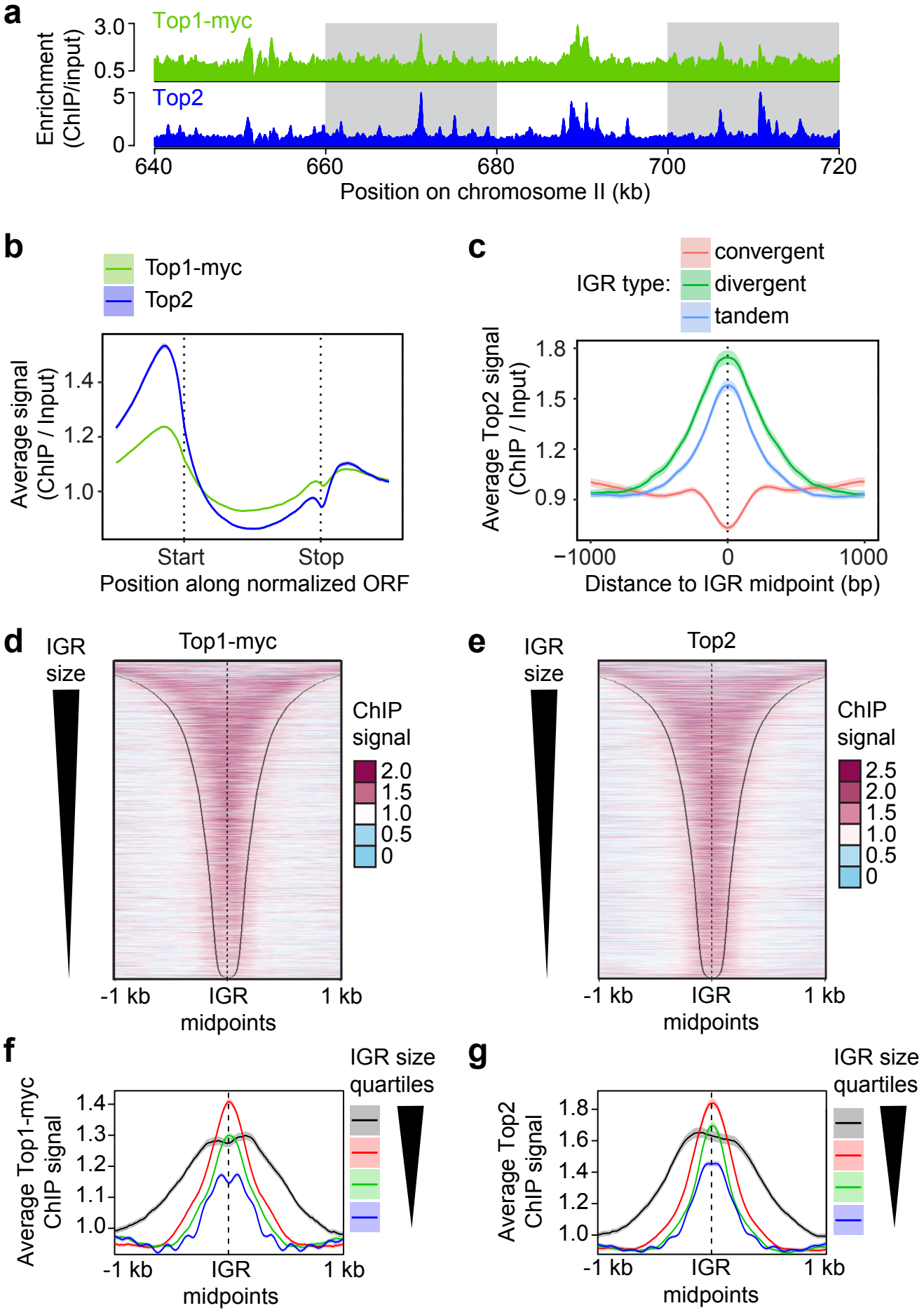

Heldrich et al., Figure 1

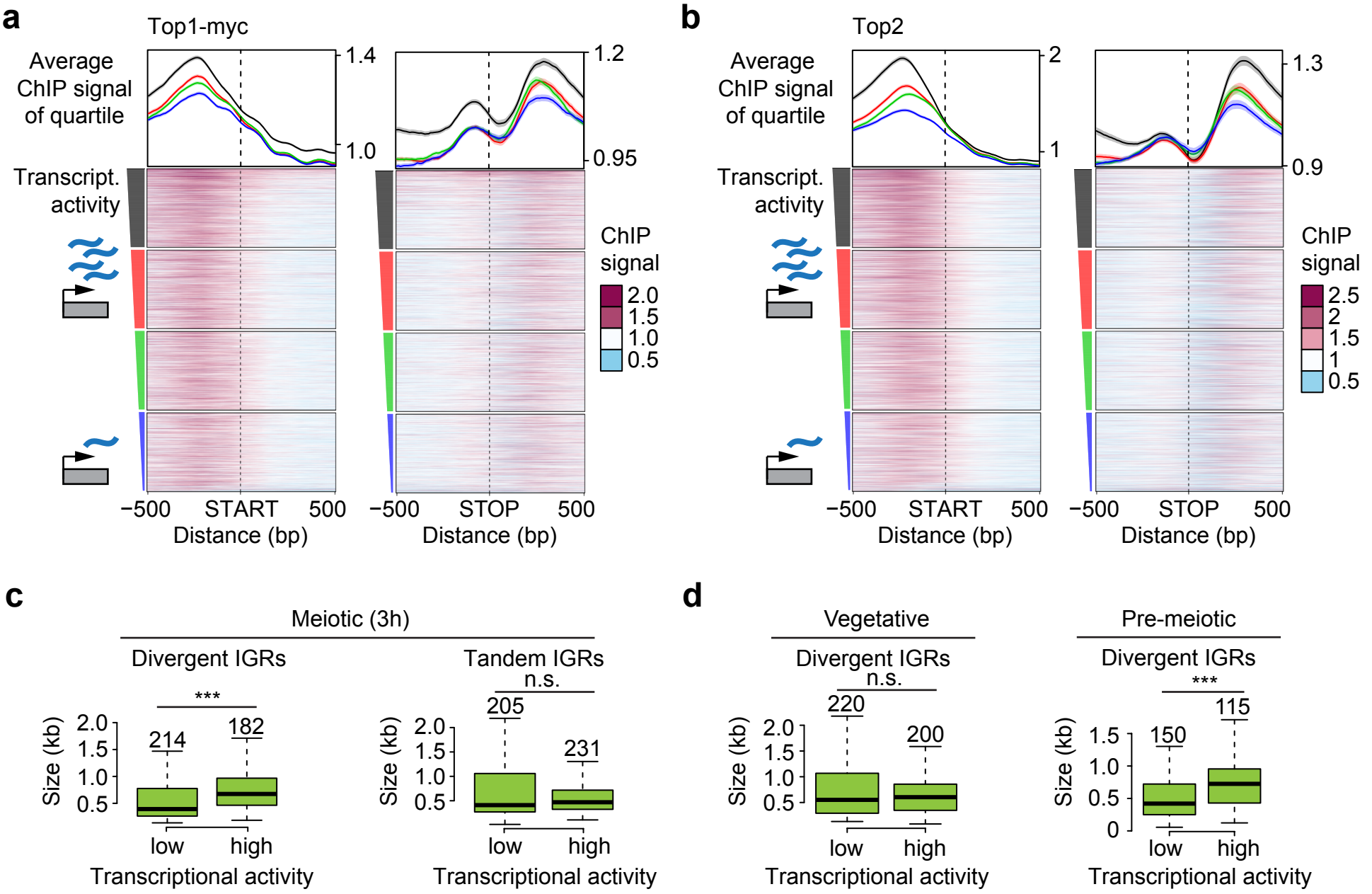

Heldrich et al., Figure 2

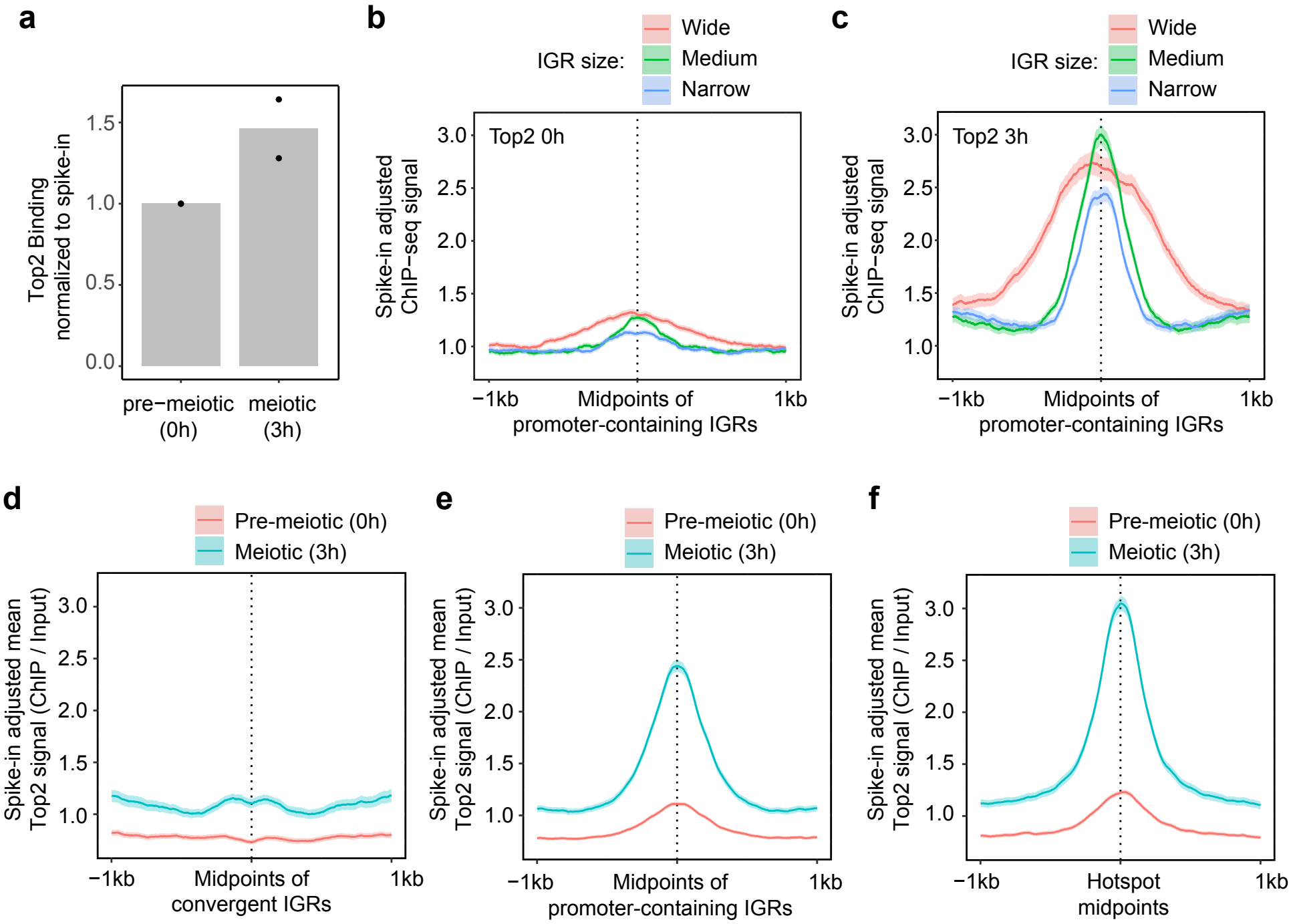

Heldrich et al., Figure 3

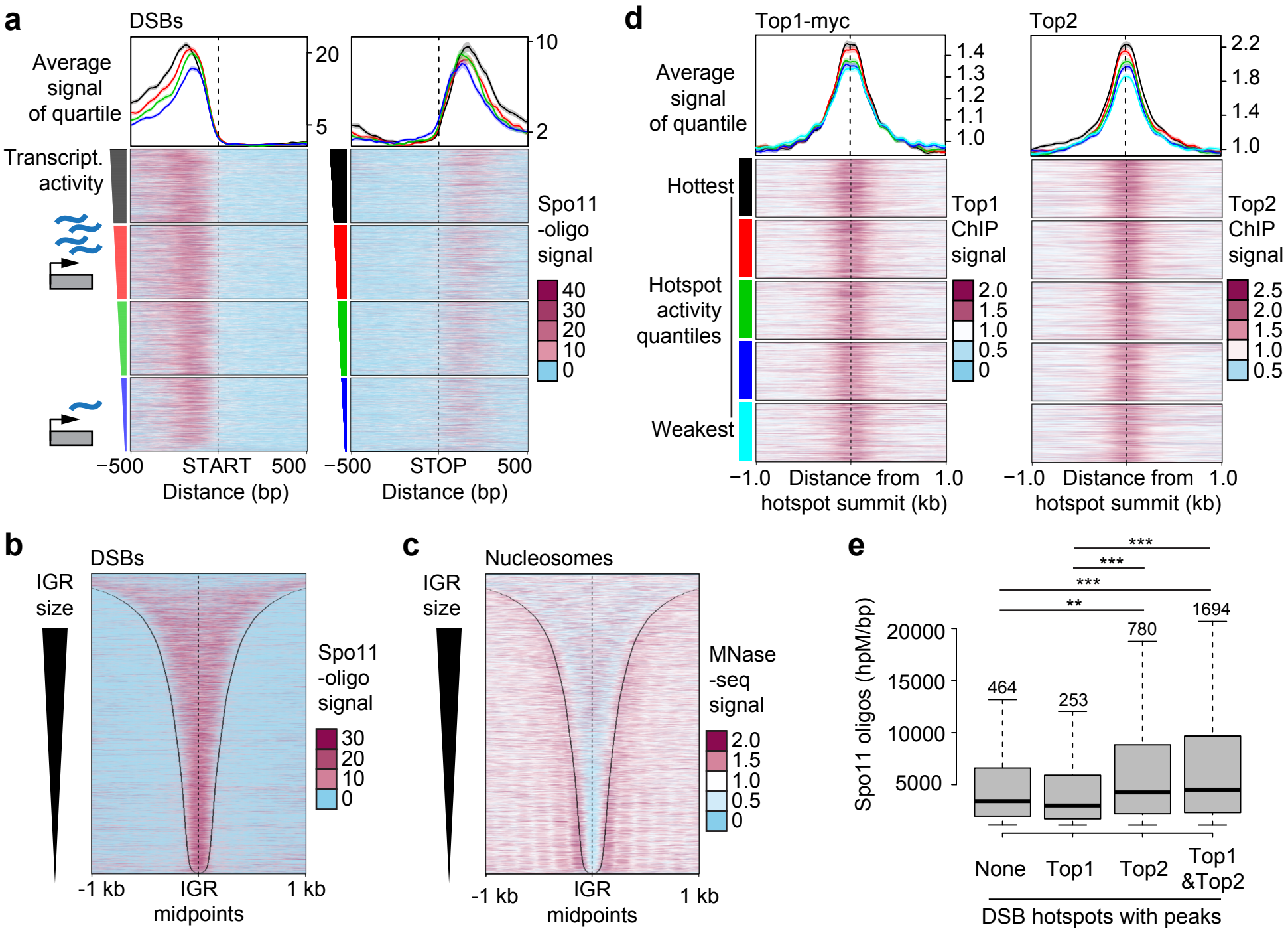

Heldrich et al., Figure 4

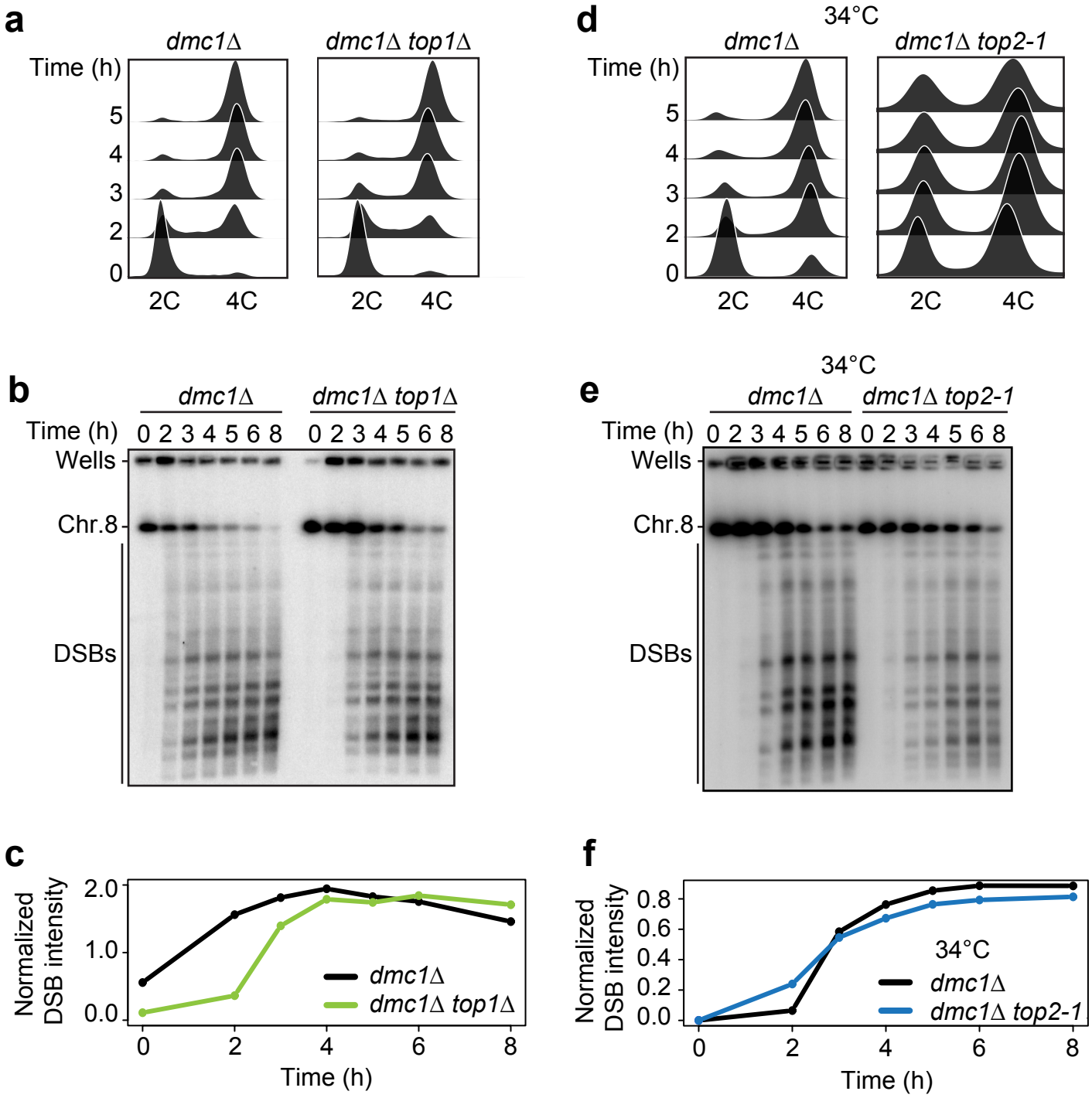

Heldrich et al., Figure 5

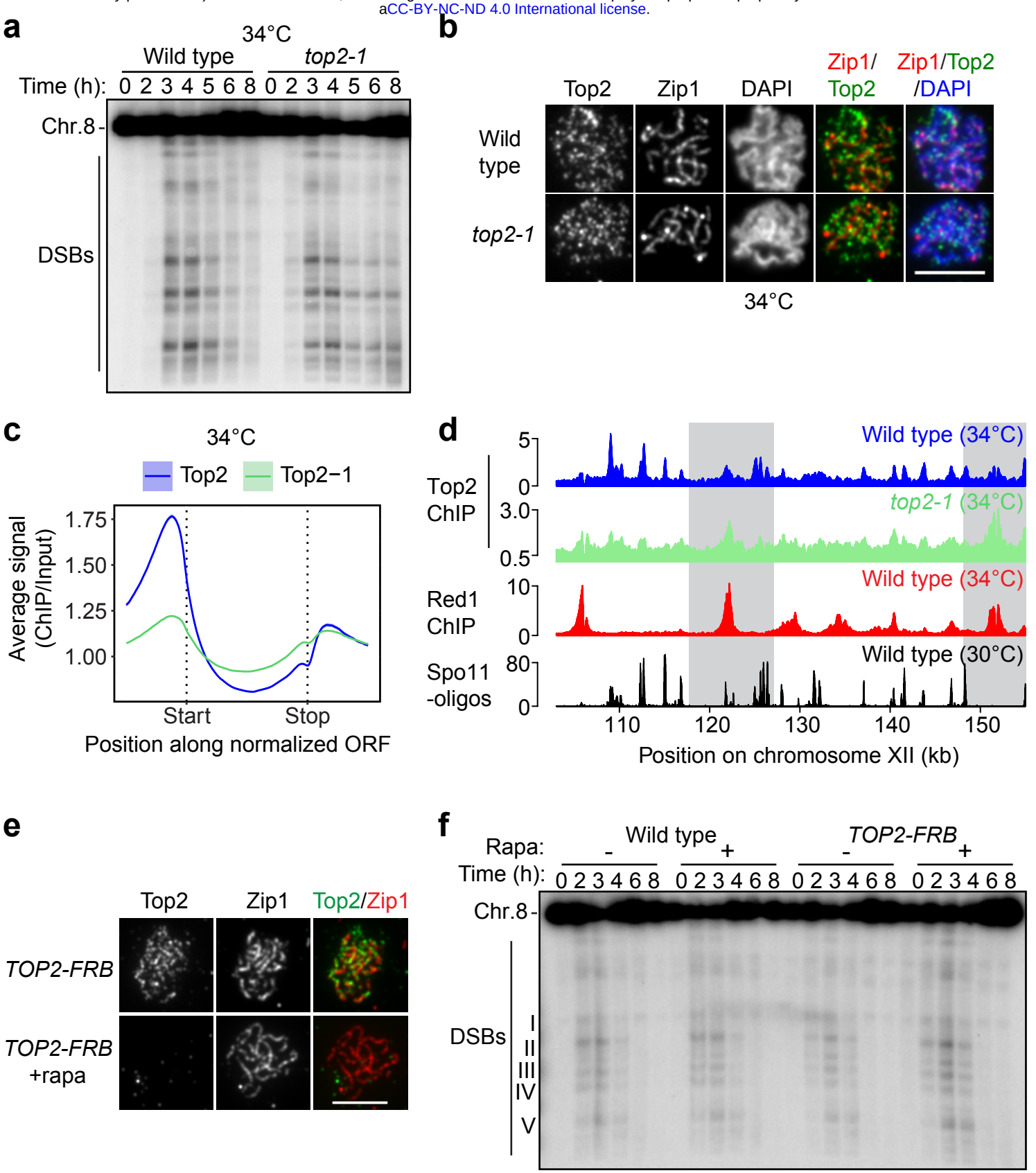

Heldrich et al., Figure 6

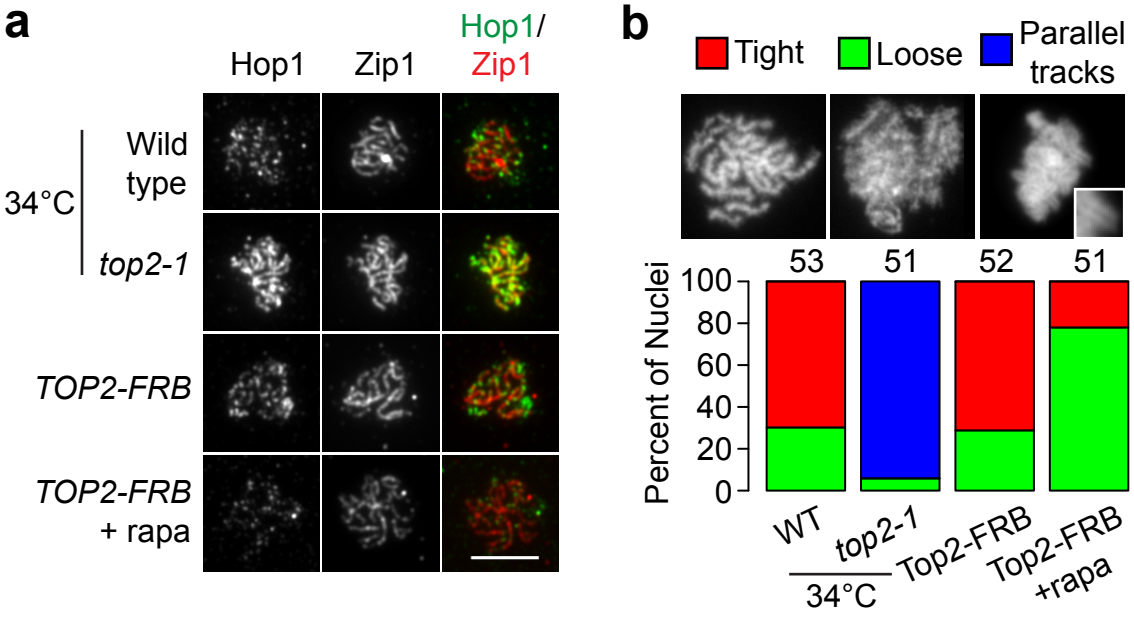

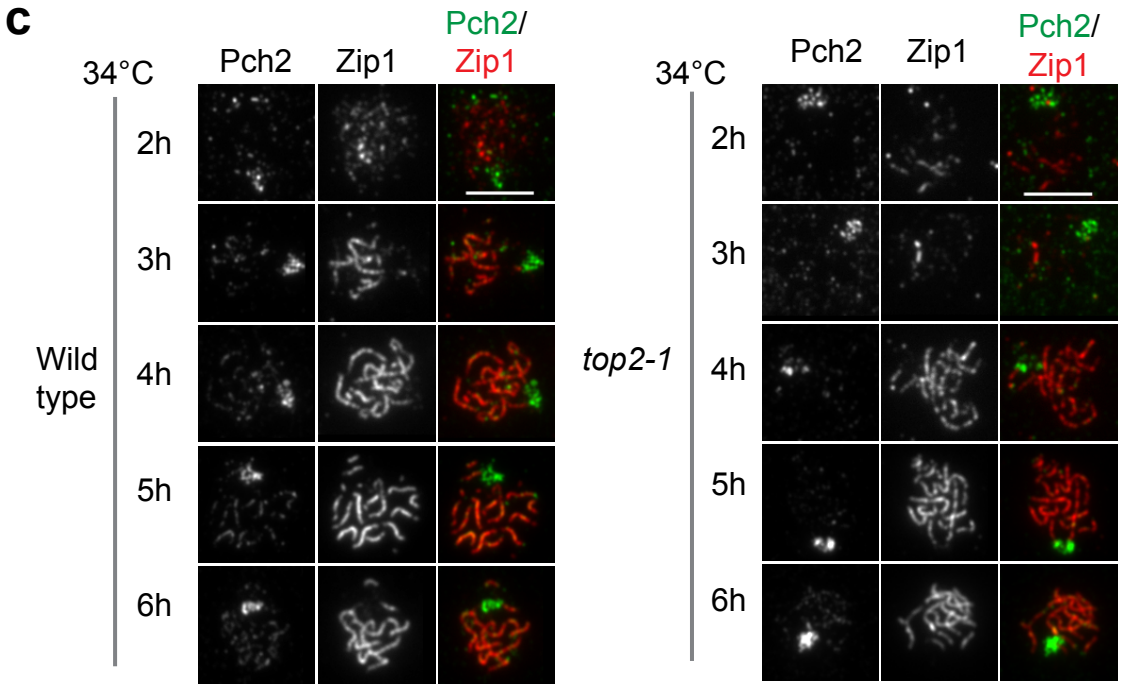

Heldrich et al., Figure 7

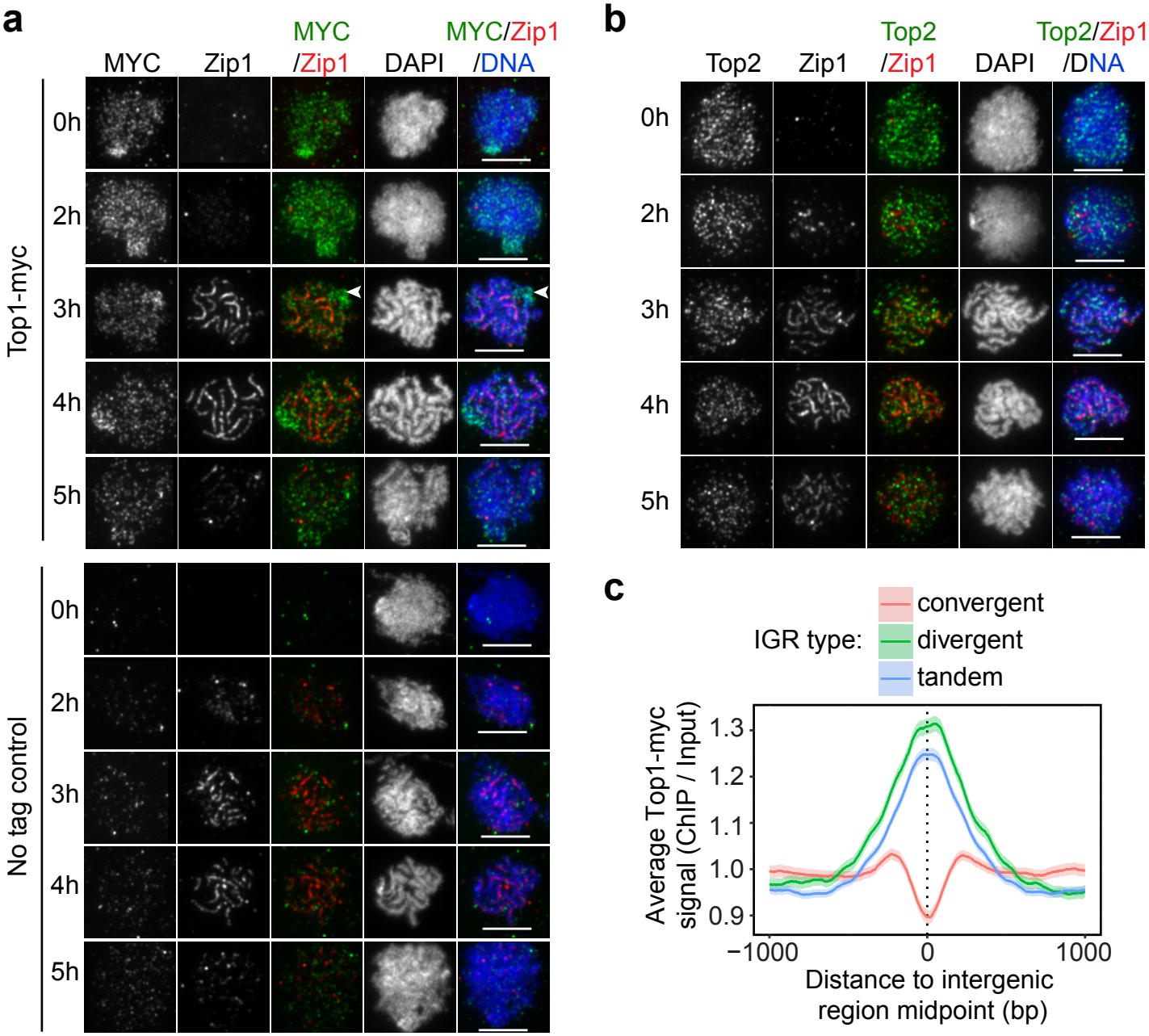

Heldrich et al., Supplemental Figure 1

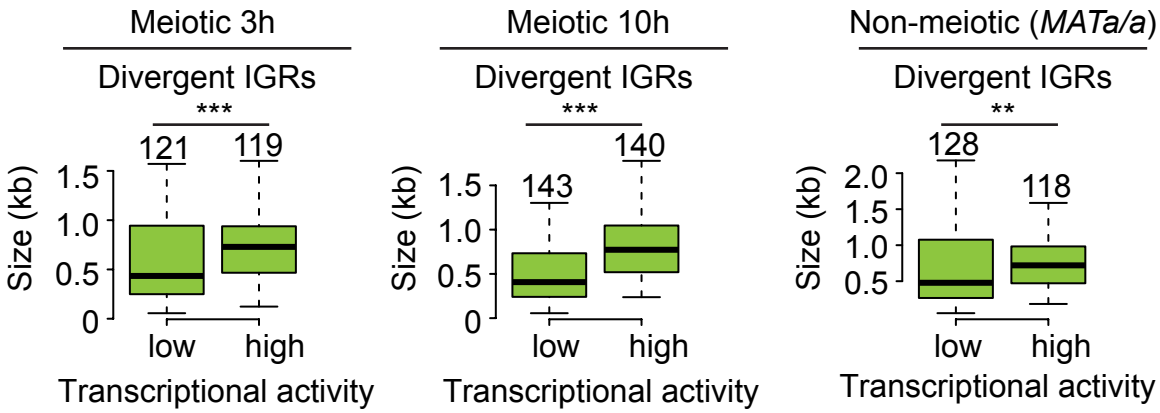

Heldrich et al., Supplemental Figure 2

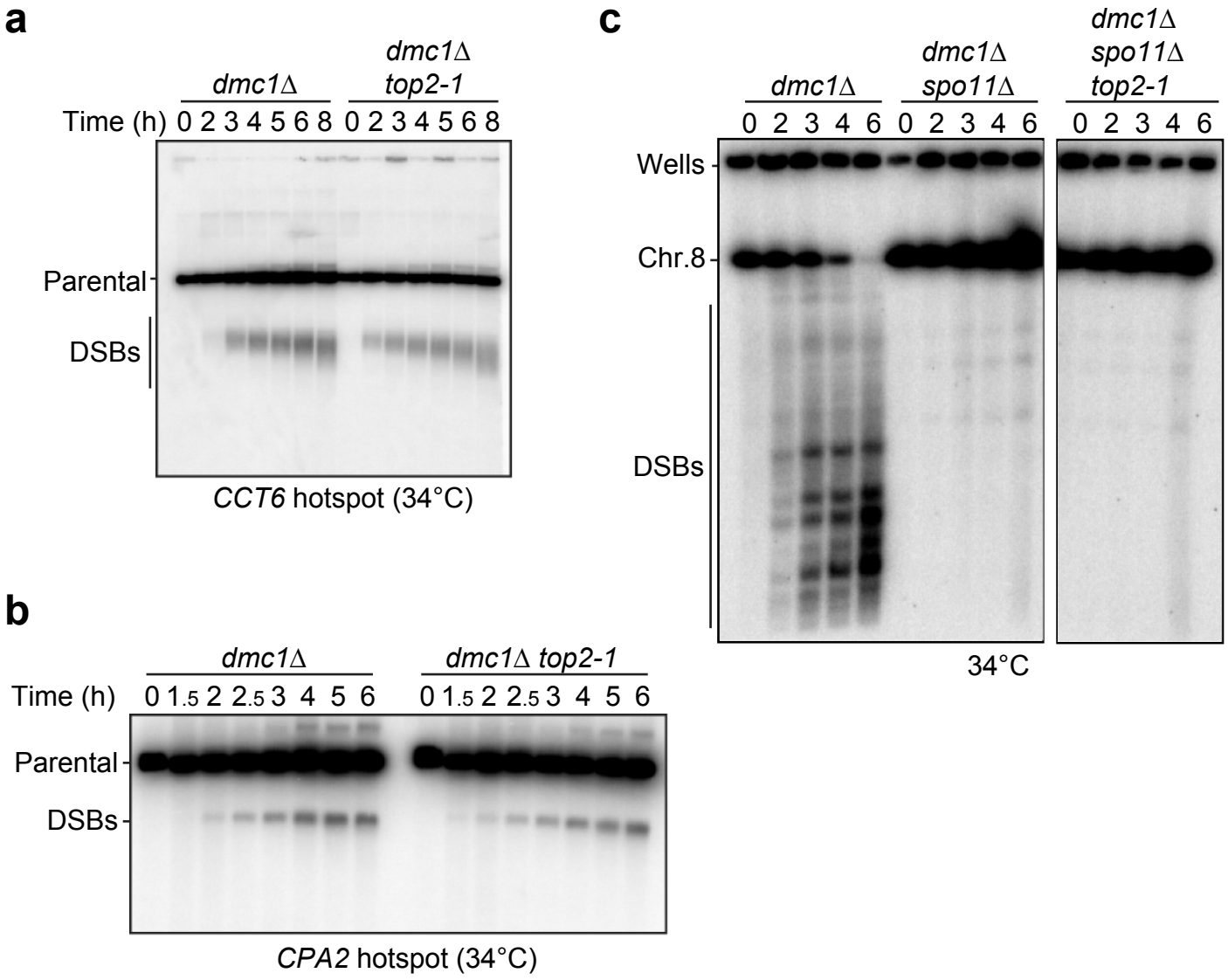

Heldrich et al., Supplemental Figure 3

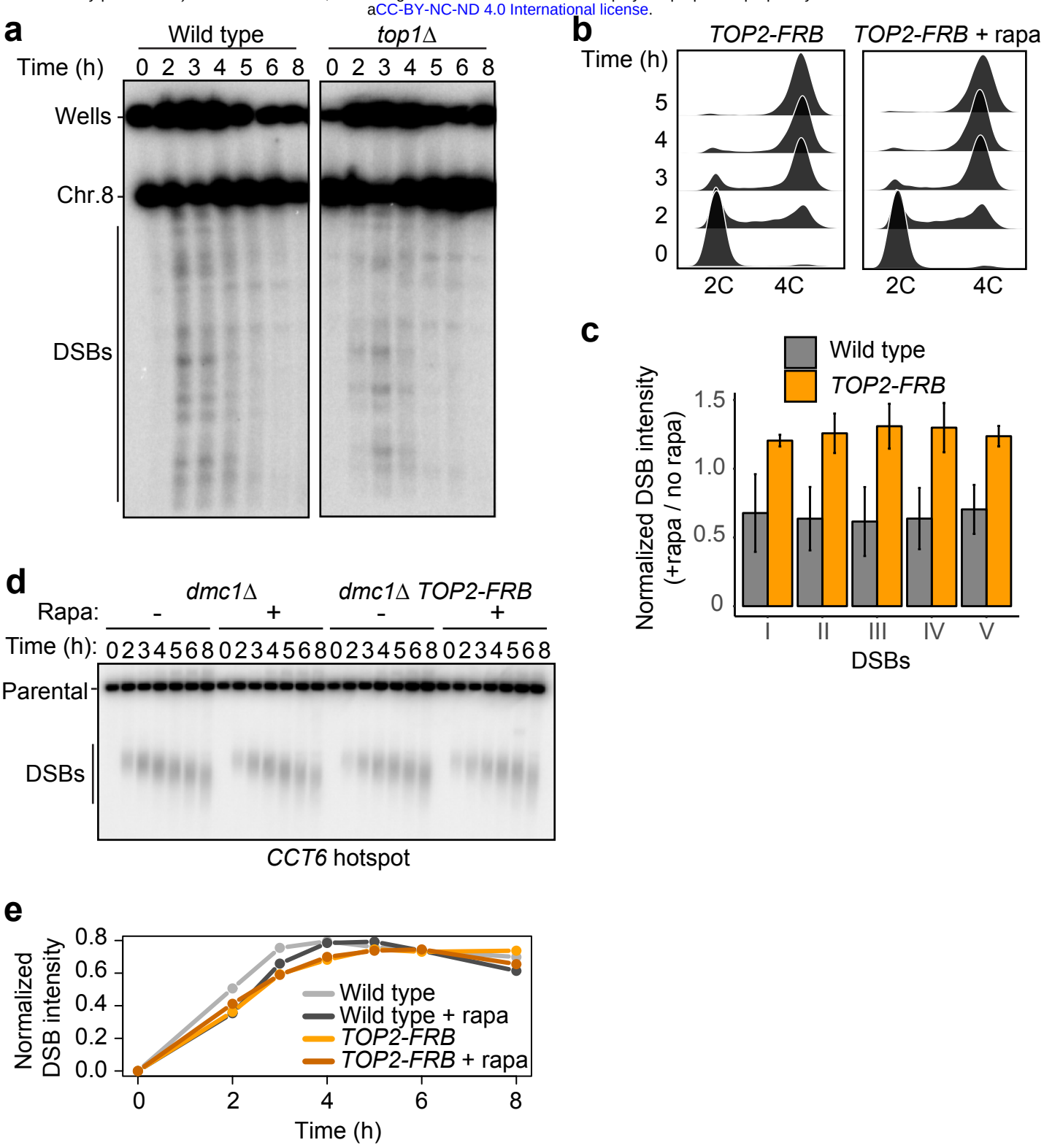

Heldrich et al., Supplemental Figure 4